Article:
Alfailakawi, M.S., Michailos, S., Ingham, D.B. et al. (2022) Multi-temporal resolution aerosols impacted techno-economic assessment of concentrated solar power in arid regions : case study of solar power tower in Kuwait. Sustainable Energy Technologies and Assessments, 52. 102324. ISSN: 2213-1388

https://doi.org/10.1016/j.seta.2022.102324

Sustainable Energy Technologies and Assessments 52 (2022) 102324

Contents lists available at ScienceDirect

Sustainable Energy Technologies and Assessments

journal homepage: www.elsevier.com/locate/seta

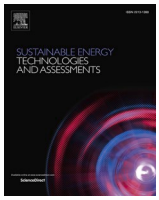

Original article

Multi-temporal resolution aerosols impacted techno-economic assessment of concentrated solar power in arid regions: Case study of solar power tower in Kuwait

Mohammed S. Alfailakawi [a,b,*], Stavros Michailos [a], Derek B. Ingham [a], Kevin J. Hughes [a], Lin Ma [a], Mohamed Pourkashanian [a]

[a] Energy 2050, Department of Mechanical Engineering, Faculty of Engineering, The University of Sheffield, Sheffield S3 7RD, United Kingdom
[b] Kuwait Ministry of Defense, P.O. Box 1170, Safat 13012, Kuwait

ARTICLE INFO

Keywords:
Solar power tower
Levelized cost of energy
Aerosols
Arid climates
Water consumption
Kuwait

ABSTRACT

This work evaluates the Solar Power Tower performance in arid regions where elevated aerosols levels and water scarcity threaten solar applications feasibility. The work conducts an aerosols aware modelling and techno-economic assessment by considering possible aerosols effects on the solar field's reflected irradiance; an effect that is typically ignored in the literature. Aerosols effect inclusion's modifies the thermal input to the solar field and this, in turn, provides a more accurate assessment. A parametric analysis has been performed using a 50 MW model by varying the Thermal Energy Storage and Solar Multiple based on three aerosols temporal resolutions: a typical year's average, daily and no-aerosols schemes. Further, water consumption is examined over four different condenser scenarios: dry, wet and two hybrid set ups. The assessment performed in Kuwait reveals that the wet-cooled condenser scenario with a 16h of storage and a solar multiple of 3.2 yields the lowest Levelized Cost of Energy of 12.06 $/kWh when the no-aerosols scheme is considered. This increases to 12.87 $/kWh when the daily aerosols are considered as the generated energy decreases by 6.7%. Besides, both hybrid condenser scenarios offer a trade-off as they result in a 55.1–68.7% of water saving for only 2.1–2.3% less energy generation.

Introduction

Since the Gemasolar Solar Power Tower (SPT) became operational in 2015, an important milestone for the Concentrated Solar Power (CSP) has been successfully achieved as the plant coupled the elevated concentration of the technology and the large Thermal Energy Storage (TES), resulting in the first CSP ever to generate electricity for 24 uninterrupted hours [1]. Also, Gemasolar was the first CSP ever to deploy molten salt as both the Heat Transfer Fluid (HTF) and a storage media which avoided having a heat exchanger between the solar field and the storage tanks, thus saving the plant capital cost and heat losses [2]. The plant has proven that the SPT technology can take a bigger share of the total CSP capacity worldwide which is dominated by the Parabolic Trough Collector (PTC) (15.3% for SPT and 76.6% for PTC) [3]. The SPT is probably one of the most efficient types of the commercially proven CSP and this is due to its high levels of concentration and elevated temperatures of the working fluid that surpasses the PTC [4,5,6]. In the SPT technology, the solar field consists of hundreds or even thousands of mirrors, called heliostats, which work on reflecting the Direct Normal Irradiance (DNI) of the sun at a common tower top mounted receiver [7].

In a typical prefeasibility research work, all CSP are observed under clear sky conditions, where the sky is cloud free and the CSP is expected to deliver its rated capacity with a focus on the DNI as it is the only solar irradiance component that can be concentrated, which qualifies it as the main design parameter for such technology [8]. However, in such sky conditions, aerosols followed by water vapor, are the most important

Abbreviations: AEG, Annual energy generation; AOD, Aerosols optical depth; CAPEX, Capital expenditures; CSP, Concentrated solar power; DNI, Direct normal irradiance; FS, Finkelstein Shafer; GHI, Global horizental irradiance; HTF, HEat transfer fluid; KISR, Kuwait institute of scientific research; LCOE, levelized cost of energy; LK, Language kit; OPEX, Operation expenditures; PTC, Parabolic trough collector; RE, Renewable energy; RTM, Radiative transfer model; SAM, System advisor model; SM, Solar multiple; SPT, Solar power tower; TAY, Typical aersols year; TES, Thermal energy storage; TMY, Typical metrological year.

* Corresponding author.
E-mail addresses: malfailakawi2@sheffield.ac.uk, m.s.alfailakawi34@kuwaitarmy.gov.kw (M.S. Alfailakawi).

https://doi.org/10.1016/j.seta.2022.102324
Received 17 January 2022; Received in revised form 18 May 2022; Accepted 22 May 2022
Available online 2 June 2022

Nomenclature

$CDF_{m(di)}$	Long term cumulative distribution function
$CDF_{y,m(di)}$	Short term cumulative distribution function
T_d	Dry bulb temperature
y_c	Aerosols post quantile mapping

Greek symbols

η_{at}	Attenuation loss [%]
η_{cos}	Cosine loss [%]
η_d	Dry cooled cycle efficiency [%]
η_{opt}	Solar field optical efficiency [%]
η_{sp}	Spillage loss [%]
ηs&b	Shadowing & blocking loss [%]
η_w	Wet cooled cycle efficiency [%]
q_{opt}	Solar field thermal power [kWh]
q_{pb}	Power block thermal power [kWh]
ϕ	Relative humidity [%]

Subscripts

A	Attenuation percentage
S	Slant range

factors that contribute to the attenuation of the DNI with a superiority of the former [9,10,11]. Other sun irradiance components, such as the Global Horizontal Irradiance (GHI) are affected by aerosols, however to a lesser extent [12]. In addition, in all CSP types, the attenuation of the DNI takes place twice, first during the transit of the sunrays towards the reflectors and secondly when the reflected rays transit towards the receiver which does not occur in other solar applications such as Photovoltaic (PV), as the sun light is harnessed once it reaches the solar panel. Aerosol extinction is best introduced by a dimensionless parameter, called the Aerosols Optical Depth (AOD) which is referred to as being the most adequate compared to any of the other parameters (e.g. Metrological Optical Range) for the purpose of attenuation measurement [13].

In contrast to all other CSP types which all have their prospective receivers within a few meters from the reflector, the heliostats in the SPT are situated at hundreds, or even thousands, of meters from the receiver, where the slant range (the distance from each heliostat to the receiver), plays a major role in the attenuation process. In the meanwhile in arid regions, where dust storms are quite frequent, aerosols can mask off up to 70% of the sun light [14]. As regards to the reflected sun rays from the heliostats towards the receiver, some researchers have found that a loss of 12.7% of the total Annual Energy Generation (AEG) can be obtained when taking into account the effect of the aerosols on the reflected sun rays [15].

Techno-Economics

Many researchers have already examined and simulated the performance of most of the CSP technologies in arid regions where solar applications are at multiple risks. Sultan et al. [16] examined the competiveness of a 50 MW PTC in Kuwait and compared its performance to a commercial operational plant in Spain. The PTC simulated in Kuwait yielded a better efficiency as the dumbed thermal energy was less. Roubiah et al. [17] examined the SPT performance in different locations in Algeria while variating the TES capacity and the solar field size which resulted in different appropriate combination based on the location's DNI resource. Also, Boudaoud et al. [18] tried to find the optimal configuration of the TES and solar field size for a SPT in different locations in Algeria, however with a fossil fuel back-up. This hybridization offered the best techno-economic returns. In addition, research has been done on comparing the SPT performance to other CSP technologies. For instance, Mihoub et al. [19] examined the performance of both the SPT and PTC at 50 MW in Algeria. They simulated different scenarios, including a fossil fuel back-up and found that the SPT with 48% back-up and a TES of 8 h is the most attractive scenario. Similarly, a comparison between the SPT and PTC has been carried out by Cekirge and Elhassan [20] in Saudi Arabia and they revealed that the SPT excels in higher efficiency and lower capital costs. Also, Hirbodi at al. [21] compared both the latter CSP types with different plant capacities, TES and solar field sizes.

Many other similar researches have been conducted in locations of interest around the world [22,23,24,25,26], however, there is no aerosols aware techno-economic assessment that exists in the literature. All previously mentioned techno-economic assessments did not consider the aerosols effect in the solar field attenuation especially that the latter can mask off up to 70% of the sun reflection towards the receiver as mentioned in the introduction. Most of the SPT techno-economic assessments are satisfied by finding an optimal combination of the key design parameters targeting the lowest Levelized Cost of Energy (LCOE) using a weather file that mainly describes the incoming irradiance but not the reflected ones towards the receiver. No techno-economic research has discussed both the effects of the aerosols on the total incoming irradiance at the solar field in addition to that effect on the reflected irradiance and the reliability of the optimal design parameter combinations in terms of the total absorbed thermal power at the receiver and the AEG. The focus of this study is to perform an accurate techno-economic assessment with the awareness of the most threatening factor of such CSP type in arid regions, i.e. aerosols (Fig. 1).

Attenuation extinction

The number of researches observing the effect of the aerosols on the reflected DNI at the SPT are constantly increasing, as more visions of Renewable Energy (RE) projects are becoming reality in the Sun Belt regions. More than six different mathematical models that describe the reflected DNI attenuation process have been proposed in the literature. The models mainly differ in the Radiative Transfer Model (RTM) used, the plant capacity/configuration and the location used for the case study. However, only a few of these models have been validated against experimental data and have shown to produce acceptable results [27]. From these mathematical models, the Polo model [15] is one of the most widely used. This model can be coupled with the transient techno-economic RE simulation tools, which enable the user to observe the projection of the effect of aerosols on the techno-economic aspects of the SPT. Using the Polo model, the difference in the AEG of a SPT with different AOD temporal resolutions has been examined. The authors simulated two extreme values of AOD, one representing an aerosols-free sky and the other a hazy sky and found that the differences in the AEG are not negligible. Furthermore, using a year of ground measured AOD data, Polo et al. [28] compared the AOD temporal resolution variation effect on the AEG of two commercial SPT plants (Ivanpah 1 and Crescent Dunes). A maximum difference of 20% has been observed in the AEG when employing daily AOD compared to the annually averaged AOD (Fig. 2).

Further, Carra et al. [29] developed a more typical representation of AOD data as they prepared a Typical Aerosol Year (TAY) in order to examine the attenuation extinction levels in Platforma Solar, Spain. This work has found that the attenuation extinction levels can reach up to 21.2% for a slant range of 2 km even when performing the simulation based on a more inclusive aerosols behavior throughout the years rather than a one-year behavior which sometimes is subject to abnormalities. Although the preparation of a more typical time period, the work did not examine the SPT outputs based on the recommended temporal resolution in arid regions, i.e. sub two days [14] and was satisfied with the annual averaged AOD. The literature still lacks a study that includes the typical behavior of aerosols, projects it at the SPT annually performance

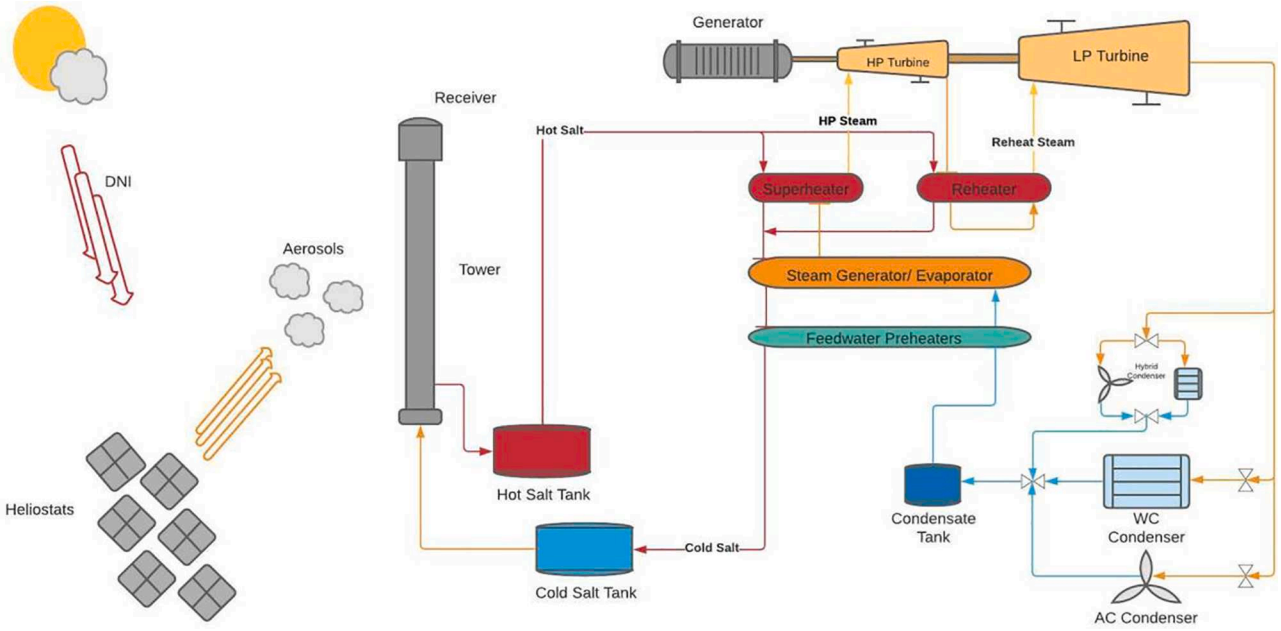

Fig. 1. Solar Power Tower diagram with 3 power block condenser scenarios.

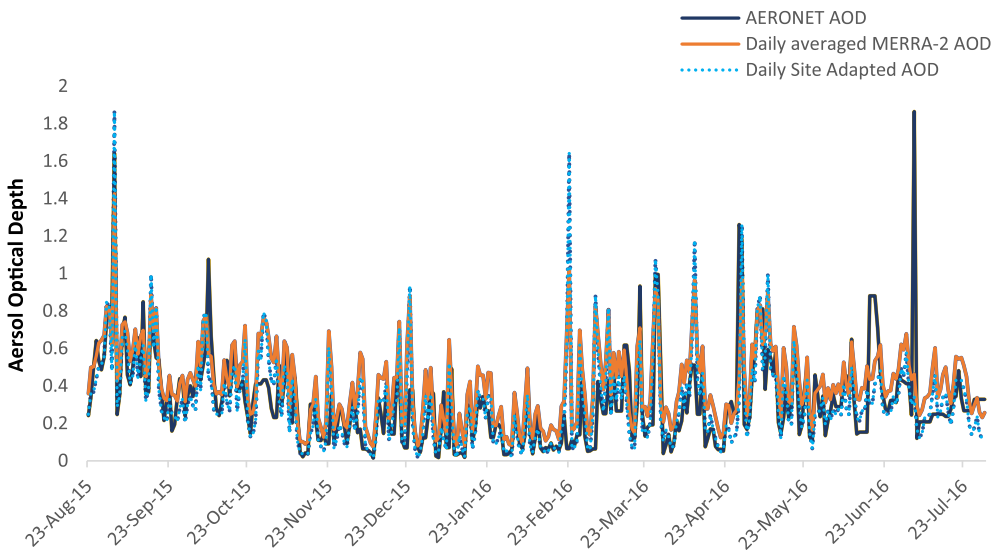

Fig. 2. A year of site adaptation by quantile mapping for the MERRA-2 AOD product in Shagaya, Kuwait.

through a techno-economic assessment and eventually examine the outputs against a fine temporal resolution.

Little information exists in the literature regarding the attenuation effect of aerosols and this has been based on examining existing commercial scale SPT plants with fixed TES and SM values in different locations worldwide [28]. This work [28] has greatly contributed in the confirmation of the aerosols effect on the reflected irradiance, however, the employed methodology assumes a fixed TES-SM configuration for different locations and this is not accurate as the optimal TES-SM depends on the DNI of the location. Thus, only a techno-economic assessment, as the one conducted herein, consisting of a parametric analysis with a variation of the main design parameters (here TES and SM) can give a much clearer understanding of how gradually a TES-SM configuration is sensitive to aerosols. In addition, the effect of the AEG reduction on the LCOE is assessed; an analysis that is missing in the literature.

Water consumption

Solar applications in arid regions raises another issue, namely the most suitable sites for the solar applications are situated in locations that lack water resources [30,31]. Water is required for cleaning the reflectors from the accumulated dust, but mainly for the heat rejection process that takes place at the condenser of the power block as the latter consumes up to 90% of the water usage in the plant [32]. Air-cooled condensers have emerged as a potential option, however with multiple penalties on capital costs and efficiency. Such a type of condenser costs up to 3 times more than the wet-cooled [33] and can result in much lower performance in hot periods of times [34], which is quite common in arid regions. The wet-cooled condenser type remains the most efficient and cost effective [35,36].

The majority of researchers have been observing both wet and dry cooled condensers in trials to find a tradeoff between the efficiency of the plant, represented by the AEG, and the economics represented by the

water consumption. For instance, Marugan-Cruz et al. [31] noticed a 3.7% decrease in the AEG when deploying an air-cooled condenser compared to a wet-cooled one. Further, Qoaider and Liqreina [37] simulated an air-cooled 50 MW PTC in Jordan and reported a decrease of only 1.5% in the AEG and an increase of 2% in the LCOE when shifting from a wet to air-cooled condenser. Fares and Abderafi [38] simulated the Noor 1 PTC plant in Morocco with an air-cooled condenser and compared the results with the existing wet one. In addition, many other researchers have examined both types from multiple prospective including exergetic analysis [39], techno-economic analysis with different types of HTFs [40], different plant capacities [21] and different locations [41]. However, much less attention has been made towards the hybrid condenser type in spite of the potential benefits that it can bring to the CSP plant, including Asfand et al. [42] who carried a thorough water consumption analysis but without a projection on the AEG or the LCOE. To the best of our knowledge, only a couple of researches have assessed the AEG using a hybrid condenser, i.e. Poullikkas et al. [33] and Wagner and Kutscher [34] and both have assumed fixed percentages of hybridization, i.e. 30 and 50%. Until now, no techno-economic assessment has been found in the literature that investigates the performance of a CSP in terms of the LCOE, AEG and water consumption with a dynamic hybrid condenser that is temperature dependent. Switching between cooling sides of the hybrid condenser based on the ambient temperature would restrict water consumption to when it is needed.

Local exploitation and incentive

Among the Middle East North Africa (MENA) region and the Arabic gulf countries of the Gulf Cooperation Council (GCC), Kuwait has recently directed its energy production policies towards the adoption of RE in order to limit its carbon emissions. It should be noted that all six gulf countries are considered among the highest fifteen carbon emitters in the world in 2009, in metric tons per capita [43]. This work also assists in giving a clearer assessment as to whether the SPT technology is an appropriate technology to fulfill the country's vision of shifting 15% of its power production towards RE by the year 2030. Further, no similar technology has ever been tested either experimentally or by simulation, while an increase in aerosols levels has been detected in the country which probably leads to a decrease in the DNI [44].

In regards to the CSP being part of this vision, the annual DNI value is found to be equal to 2100 kW/m^2/y in approximately most of the Kuwait land area [45], which is known to be sufficient for such a technology [5,8]. A resources assessment has elected CSP as a high potential technology to be implemented in Kuwait [46] based on the elevated levels of the DNI in the country, however, elevated levels of aerosols are also recognized and considered as a concern for such technology [47,48]. The first phase of the vision has been already accomplished in the western part of the country at the Shagaya Renewable Energy Park where a 50 MW PTC, a 10 MW PV and a 10 MW wind farm are already in operation. A total of 4 GW is projected to be generated by RE according to this vision including 1.15 GW for CSP where the SPT has a share, however with, as yet, no assigned capacities or configurations [49,50].

Aim and objectives

The main aim of this work is to assess the techno-economic feasibility of the examined technology in such extreme weather conditions as that of the case study location. To accomplish this, firstly, all the possible effects of aerosols must be carefully observed and quantified. Then, the aerosols effect must be included with multi temporal resolutions into the techno-economic assessment (a wide range of TES-SM has been considered). This will assist in examining how gradual is the effect of aerosols over the increasing SM range and how is the role of the TES in the compensation of the AEG potential losses.

The techno-economic assessment essentiality emerges from the fact that some arid regions with elevated levels of aerosols might appear as inappropriate for such technology only because the aerosols effect is amplified when coupled with a large solar field. An aerosols impacted techno-economic assessment, as the one proposed in this paper, would give an appropriate solar field size, larger than which the effect of aerosols will have a considerable amplified impact due to the too large slant ranges. Thus, a novel fully aerosols aware method of conducting a techno-economic assessment in arid regions is proposed in this work for the SPT technology. The method considers all possible effects of aerosols on such technology, namely, the total incoming irradiance on the solar field, the reflected irradiance in addition to the aerosols temporal resolution variation effect. In addition, a water consumption analysis is carried out in this paper that includes wet, dry and two hybrid condenser set ups. This is mainly realized through the following objectives:

- Assembly of a site adapted Typical Aerosols Year.
- A parametric analysis of the key design parameters that lead to the lowest LCOE for different types of power block condensers.
- An examination of different aerosols temporal resolutions employment effect on the outputs of the parametric analysis optimal design parameters combinations.

Materials and methods

Metrological data

Typical metrological year (TMY)

As part of the solar resources evaluation in Kuwait, the Kuwait Institute for Scientific Research (KISR) has obtained at least one year of ground measured data at five potential sites in Kuwait [47]. The most interesting site among the five locations, i.e. Shagaya, has been already set with a TMY weather file that is based on site adapted satellite derived data acquired from SolarGIS. The TMY is obtained based on typical values of the most important weather parameters in the period between 1999 and 2016 and has been provided to the authors by KISR.

Typical aerosols year (TAY)

Supervised by NASA, KISR has also managed to set the site of Shagaya with an Aerosol Robotic Network (AERONET) station from which the short-term ground measured AOD data, has been acquired. The latter data is for 289 days, a little longer than the minimum mandatory period for ground measured data in a site adaptation process, i.e. nine months [51,52]. In addition, the latter data lies in the same period as the TMY from KISR, i.e. 2015–2016. This data has been specifically chosen due to its high quality (level 2) which is known to be the most reliable data offered by AERONET as it is cloud screened and controlled data [53].

For a more typical aerosols behavior, the short-term ground measured AOD data from AERONET has been used in a site adaptation process with a long-term AOD data acquired from the reanalysis model of the Modern-Era Retrospective analysis for Research and Applications Version 2 (MERRA-2) which is highly referenced and widely used. The reanalysis model provides AOD data, besides several atmospheric parameters, through assimilation in a global forecast model, i.e. GEOS with a spatial accuracy of 0.625° x 0.5° and with a temporal resolution of 1-hourly [54]. The location of interest here is determined by a bounding box, which corresponds to the location of Shagaya, i.e. (47.060306°W/29.209889°S/47.160306°E/29.309889°N).

The site adaptation has been realized by the quantile mapping technique which insists on the establishment of a quantile dependant correction function that decreases the difference between both data sets, i.e. the cumulative distribution function of the modelled data (CDF_m) and it is matched to the one of the observed data (CDF_0) [55]. The technique is considered as reliable and widely used in the literature [56,57], and has managed to reduce the existing bias between the ground measured data of AERONET and the corresponding data of MERRA-2 over the same period as the mean bias deviation has decreased

from 0.1 to −0.0001 and the root mean square deviation decreased from 0.21 to 0.206. The slight improvement in the bias reduction is mainly due to the high-quality reanalysis model data of MERRA-2.

This technique uses the CDF as an operator that results in quantiles of data and in order to accomplish the latter, a vector of quantiles must be assigned for each data set through their prospective CDFs, i.e. CDF_0 and CDF_m. The interpolation of the new corrected values (y_c) is obtained using the inverse of the CDF_0 as an operator as follows:

$$y_c = CDF_0^{-1}[CDF_m(x_m)] \quad (1)$$

This procedure has been carried out using five years of MERRA-2 data in the period between 2012 and 2016 which also intersects with the year of the ground measured data (2015–2016) of AERONET. The period of five years is sufficient for this purpose according to several researchers and has been used in [58] and [59]. The long-term data is for capturing the inter-annual and seasonal changes. These long-term data sets, whether ground or satellite measured, are converted into the most typical form of representation, i.e. TAY. For each accounted metrological parameter, each individual month from different years is compared to the long-term behaviour of the parameter, and the closest month is selected as a candidate month, thus forming a typical year. The most common method in the literature is the Sandia Method [60] and this is followed by the NREL method [61]. Both methods use the Finkelstein-Schafer statistics (FS) technique to measure the closeness of the short-term behaviour (each individual month) to the long term one (every similar month along the entire data period). The FS is obtained as follows [29,62]:

$$FS = \frac{1}{N}\sum_{i=1}^{N}|CDF_{m(di)} - CDF_{y,m(di)}| \quad (2)$$

where $CDF_{m(di)}$ is the cumulative distribution function of the long term of the indices (d_i) daily mean, $CDF_{y,m(di)}$ is the cumulative distribution function of the short term in month m and year y and N is the days number in the corresponding month (in order to normalize the FS for months with different number of days [63]).

Both CDFs are first calculated by taking the daily means of the hourly values in the entire study period for each of the indices. Then, the daily means are sorted in ascending order in order for the CDF to be calculated based on the rank $K(i)$, $j(i)$ of the specific unrepeated value (i) and the number of days in the corresponding month N, the number of days in any calendar month of the entire data set n as follows [64]:

$$CDF_{m(di)} = \frac{K(i)}{N+1} \quad (3)$$

$$CDF_{y,m(di)} = \frac{j(i)}{n+1} \quad (4)$$

As a result of applying the FS statistics, the typical year is constructed by typical months from different years, e.g. January from the year 2012 and February from 2013, as presented in Fig. 3.Fig. 4..

Further, once the TAY is assembled according to the Sandia Method, the selected months from different years are concatenated in a daily AOD basis in order to test the temporal resolution variation effect on the plant's outputs. However, the yearly averaged AOD value of the assembled TAY is still of importance for the preliminary evaluations of the parametric analysis which targets the optimal TES-SM combinations based on the lowest LCOE. Here, the annual averaged AOD value based on the site adapted TAY is equal to (0.3205).

Solar power Tower performance

System advisor model (SAM)

The System Advisor Model (SAM) is a simulation tool developed by the National Renewable Energy Laboratory (NREL) and supported by the United States Department of Energy (DOE) [65]. SAM, which is freely available, includes a SPT performance model among multiple RE models, e.g. PTC, Linear Fresnel Reflectors, Solar Power Dish, wind and PV [66]. An advantage offered by the SAM is that it incorporates not only the technical aspects of the simulated plant performance but also the financial aspects.

The tool is capable of performing a series of steady state solutions at hourly intervals that can approximate a transient system over the course of a year, and this can assist the user to observe the evolution of both the technical and economic parameters on an hourly resolution of the entire year. SAM works on the reading and processing the user inputs and specified weather file data, finds iterative solutions of the system and finally converges [67]. The dynamism of the tool is based on finding solutions for the time varying HTF flow and heat transfer variables in addition to constant inputs at each time step of the hourly weather file of the TMY (i.e. 8760 h). For that, the tool implicitly runs multiple steady state iterative simulations, which are proper to the actual time step. Once the convergence is reached for a given time step, the solution of the actual time step becomes the previous time step solution for the next time step. Such a simulation process is necessary in order to examine the parameters evolution over time, which is essential for an accurate solar radiation simulation. It is worth mentioning that in addition to the DNI values (which are essential for a CSP performance model), the tool calculates the sun position based on the location's coordinates existing at the weather file and thus the solar rays directions and the solar field optical efficiency.

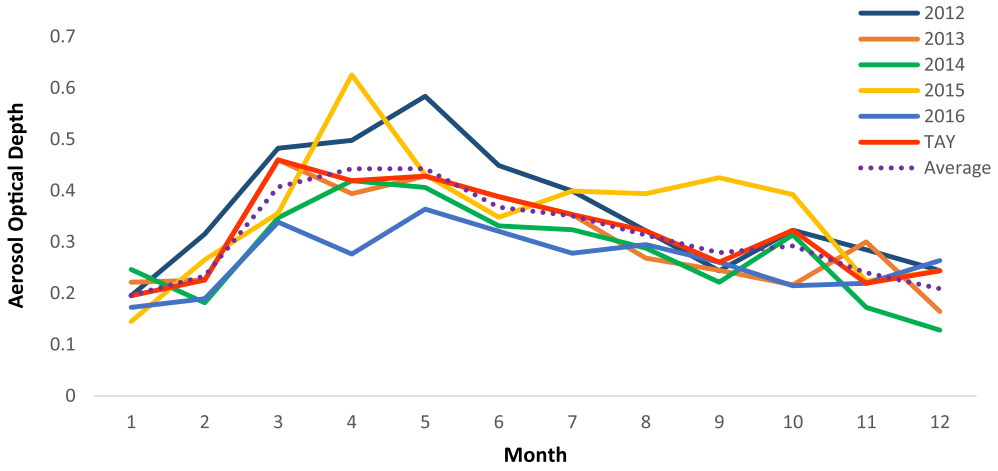

Fig. 3. AOD month selection for the TAY assembly according to the Sandia Method.

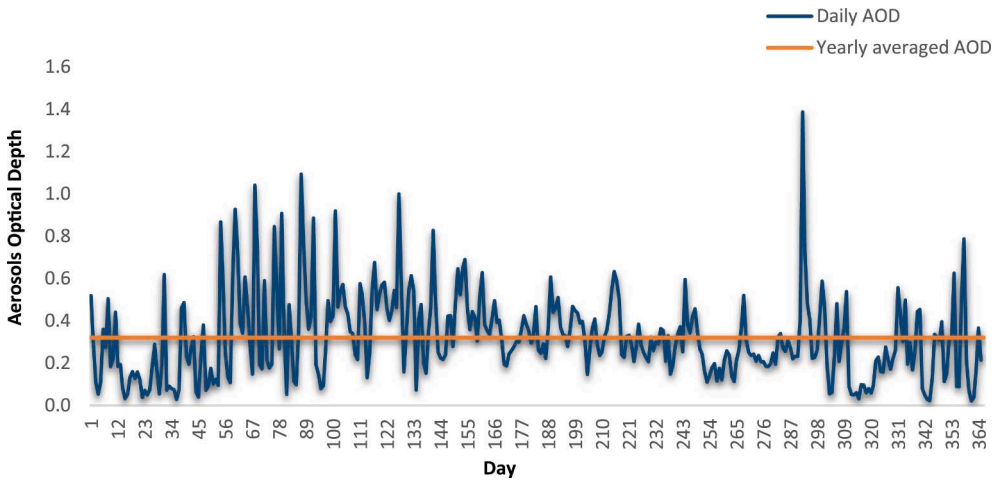

Fig. 4. The TAY daily and annually averaged AOD behaviours.

Further, SAM incorporates multiple specific tools that automatically optimize key design parameters in the plant once enabled by the user. For instance, the SAM's SPT performance model integrates a separate tool which assists in the tower and receiver characterization process, ray tracing and heliostats positioning, i.e. SolarPILOT, which has also been developed by NREL and can be used as a stand-alone tool [68]. The tool calculates the incident thermal energy of the solar field as follows [69]:

$$Q_{Field} = N_{hel}.A_{hel}.DNI \tag{5}$$

where N_{hel} is the number of heliostats and A_{hel} is the area of a single heliostat. In addition, the tool consists of a weather attenuation loss evaluation function , and this includes the attenuation effect in the solar field efficiency calculation as follows:

$$\eta_{opt} = \eta_{\cos}.\eta_{at}.\eta_{sp}.\eta_{s\&b} \tag{6}$$

where η_{cos} is the cosine loss, η_{at} is the attenuation loss, η_{sp} is the spillage loss, $\eta_{s\&b}$ are the losses due to the shadowing and blocking [70,71]. This results in the incident thermal energy at the receiver being affected by the solar field optical efficiency as follows [72]:

$$Q_{rec} = A_{hel}.N_{hel}.DNI.\eta_{opt} \tag{7}$$

Due to the reasons mentioned earlier in the introduction concerning the attenuation extinction of the SPT, SAM deploys a unique weather attenuation loss evaluation function and this is in the SPT performance model. The function is in the form of a third order polynomial with regards to the slant range (S), i.e.:

$$A(\%) = aS^3 + bS^2 + cS + d \tag{8}$$

where A is the attenuation percentage. The four coefficients in the polynomial are unique functions of the slant range and the (x,y) positions of each heliostat in accordance with the sun and the receiver, hence an annual mean loss percentage is calculated by the SolarPILOT [65]. This can lead to the incorrect estimation of the model performance because of two aspects: first, no aerosols effect on the reflected irradiance is included despite its potential influence. Second, the aerosols have a very high degree of spatiotemporal variability [73] and cannot be accurately described by an annual attenuation function. Thus, the introduction of the aerosols effect, in addition to the effect of the distance with the recommended temporal resolution on the attenuation function of the solar field must be much better understood.

Polo model

Among the very few other researchers that have developed a solar field attenuation model, Polo et al. [15] has used a RTM, namely the Libradtran, in order to develop an AOD dependent attenuation model. This enables the accurate determination of the four coefficients in the third order polynomial for the heliostats field's weather attenuation function used in SAM. This model is reportedly referred to as very promising extinction model for SPT plants [27] and with the assistance of this model, an integrated effect of both the slant range and aerosols is obtained in the solar field weather attenuation function. The model is uniquely appropriate to AOD wavelengths of 550 nm and slant ranges up to 3 km. These coefficients are given as follows:

$$\begin{aligned} a &= 3.13AOD^3 - 1.9AOD^2 + 1.6AOD - 0.133 \\ b &= -14.74AOD^3 + 2.49AOD^2 - 11.85AOD + 0.544 \\ c &= 28.32AOD^3 - 7.57AOD^2 + 48.74AOD + 0.371 \\ d &= -2.61AOD^3 + 3.70AOD^2 - 2.64AOD + 0.179 \end{aligned} \tag{9}$$

In addition, SAM incorporates a scripting language, namely (LK), which enables the user to run more advanced customized simulations, i.e. input automation based on user developed scripts. Parametric analyses can be carried out based on multiple runs with a user specified step size and number of iterations. This gives the user a better insight of the parameters variation effect on the performance of the simulated technology with ease and much savings in time. SAM also employs another scripting tool, namely the Software Development Kit (SDK) which permits the user to develop scripts and take over the performance model out of the SAM simulation core using other languages, e.g. C/C++, JAVA, Python [74].

Parametric analysis

A parametric analysis has been carried out for two key design parameters: The Thermal Energy Storage capacity (TES) and the Solar Multiple (SM) in order to observe the variation effect of such parameters on the important plant outputs. The analysis targets the lowest LCOE as an indication of an optimal TES-SM combination. The TES is where all the excess heat of the solar field is stored and it is varied from 0 h to 18 h with a step size of 1 h. The SM is the ratio of the thermal power produced by a specific solar field size at the design point to the power required at the power cycle block at nominal conditions [2]. In other words, a SM of 1 basically represents a solar field size with which the plant will deliver its full power directly to the power block with no excess power (dedicated to co-generation or TES for example). While a SM of 2 can provide the full power required at the power block as well as an equivalent amount of power to the TES for later usage. The SM is given by [18]:

$$SM = \frac{Q_{sf}}{Q_{pb}} \tag{10}$$

where Q_{sf} is the thermal power from the solar field and Q_{pb} is the thermal

power to the power block. Here, the SM ranges from 1 to 4 with a step size of 0.2. A total of 304 simulations have been performed for each type of condenser using the inputs shown in Table 1.

Due to the limitations in the published technical data of CSP in Kuwait, the examined SPT plant is assumed to have 50 MW in order for it to be comparable to the only operating CSP plant in Kuwait, i.e. Shagaya 50 MW PTC. This capacity has been revealed as a potential standardized CSP capacity [75,76].

Power block condenser scenarios

In addition to the better heat rejection that wet-cooled condenser can import to the steam Rankine cycle compared to the air-cooled condenser due to the higher heat capacity [77,78], the latter type is usually of a bigger initial costs [33]. However, the scarcity of water in arid regions forces the users to limit their usage of water to the lowest necessary quantities. A small water requirement in the case of CSP is used for the mirror washing (1.4%). This cannot be replaced (air cleaning is less effective and is not available in the SAM), while the biggest amount of water is for the heat rejection at the condenser (90%) [79] and can be replaced by using an air-cooled condenser which uses air for heat rejection despite not being as great conductor [80]. A hybrid condenser option including both wet and dry condensers mounted in parallel can take the advantage of the wet-cooled side's better heat rejection as well as the lower water consumption of the air-cooled side.

In a conventional Rankine cycle based on a dry cooled condenser, the only variable that has an effect on the cycle performance is the dry bulb temperature (T_d). The efficiency of the dry cooled cycle is shown as follows [81]:

$$\eta_d = -0.1468T_d + 22.526 \quad (11)$$

In addition, as the difference between the wet and dry bulb temperatures depends on the humidity in the air (wet and dry bulb temperature are equal at 100% humidity [82]), in the wet-cooled condenser cycle, both dry bulb temperature and the relative humidity are of importance and considered in the wet-cooled cycle as follows:

$$\eta_w = a(\phi)T_d + b(\phi) \quad (12)$$

where ϕ is the relative humidity, and a and b can be obtained as follows:

$$a(\phi) = -0.102\phi - 0.0684 \quad (13)$$

$$b(\phi) = -0.305\phi + 24.26 \quad (14)$$

The SAM enables the user assigning the temperature at which the power cycle is supposed to operate at its rated efficiency, i.e. the ambient temperature at design. The latter must be a dry bulb temperature in the case of air-cooled condenser, and a wet bulb temperature in the case of wet-cooled condenser [81,83]. In this work, the design temperatures shown in Table 1 are the average wet/dry bulb temperatures from March to September and they are taken from the weather file as it is the period at which CSP are expected to deliver its highest production [31].

Several researchers have observed an efficiency drop in the power block with air-cooled condenser at temperatures above 32 °C and a serious efficiency drop at temperatures above 37 °C [32]. Thus, in this paper the hourly scheduling set up in the SAM system control has been automated in accordance with the monthly averaged dry bulb temperature of the weather file. As in the case when the temperature is below 32 °C (or 37 °C), the air-cooled side of the hybrid condenser is activated, while in the case when the temperature is higher than 32 °C (or 37 °C), the wet-cooled side is activated. Two different scenarios have been initially considered based on the latter reference temperatures, i.e. wet-cooled side activated in months with average temperatures equal or above 32 °C and wet-cooled side activated in months with average temperatures equal or above 37 °C.

The hot arid climate of Kuwait resulted in only two months (July and August) having a monthly average temperature higher than 37 °C, which represents 17% of the year time. The second scenario is based on activating the wet-cooled side of the condenser in case the monthly temperature averages are higher than 32 °C and this has been found in five months (May to September) which represent 42% of the year. However, the inclusion of the entire month is misleading as some temperatures drop over the night of the above mentioned months have been observed, and this is shown in Fig. 5.

Thus, for a more accurate simulation, the system control has been set based on each hourly averaged temperature for each month and this is shown in Fig. 6, which results in having only 19% of the temperatures above 37 °C while 30% are higher than 32 °C, hence the hybrid scenarios are named accordingly. In Fig. 6, the digit 1 indicates when the wet-cooled side activation, while the digit 2 indicates the activation of the air-cooled side of the hybrid condenser.

Table 1
SPT technical parameters.

	parameter	description
System Design	Solar multiple	1 to 4 (with a step of 0.2)
	Irradiation at design	700 W/m^2
	HTF hot temperature	574 °C
	HTF cold temperature	290 °C
	Full load hours of storage	0–18 (with a step of 1 h)
Tower and Receiver	Tower height	Obtained from optimization (SolarPILOT)
	Receiver diameter	Obtained from optimization (SolarPILOT)
	HTF type	Molten Salt (60% $NaNO_3$ + 40% KNO_3)
	Receiver flow pattern	Configuration 2
Heliostats Field	Layout configuration	Always optimize
	Heliostats length	12.2 m
	Heliostats width	12.2 m
	Water usage per wash	0.7 L/m^2
Atmospheric attenuation	Annual averaged AOD	0.3205
	Polynomial coefficient 0	−0.0037298
	Polynomial coefficient 1	0.154
	Polynomial coefficient 2	−0.0348
	Polynomial coefficient 3	0.0028768
Power Cycle	Condenser type	Air-cooled, wet-cooled and Hybrid
	Ambient temperature at design	31.6 °C for the air-cooled and hybrid condensers 14.3 °C for the wet-cooled condenser
Thermal Energy Storage	Storage type	Two tanks
	Tank height	20 m

AOD temporal resolution variation

Despite the integration of the aerosols effect in the solar field mentioned in sections 3.2.1 and 3.2.2, the polynomial coefficients are still based on a yearly averaged AOD value. This is because it is the conventional set up in the SAM, as well as all other RE simulation tools and this is not the temporal resolution that has been recommended by lead researchers, i.e. sub two days [14], in order to avoid the effect of the high spatiotemporal variability of the aerosols, especially for arid regions. This has led Polo et al. [28] to use the Polo model (equation (9)) but with an automation applied on the SAM. The authors performed the automation with the assist of the SDK tool, which is offered by the SAM, and this enabled the simulations to be performed based on the number of AOD values, i.e. 12 and 365 (for monthly and daily AOD resolutions). This process creates 12–365 polynomials, hence a similar number of solar field attenuation scenarios for the same solar field. The current

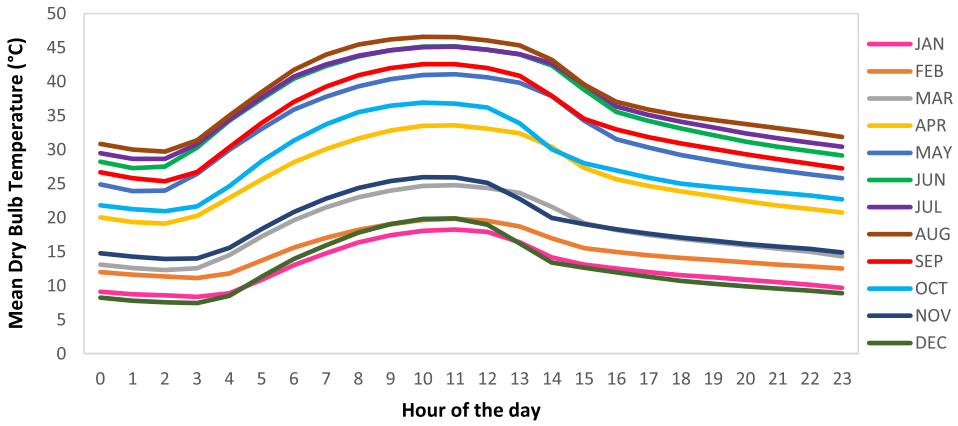

Fig. 5. Monthly averaged dry bulb temperature at Shagaya.

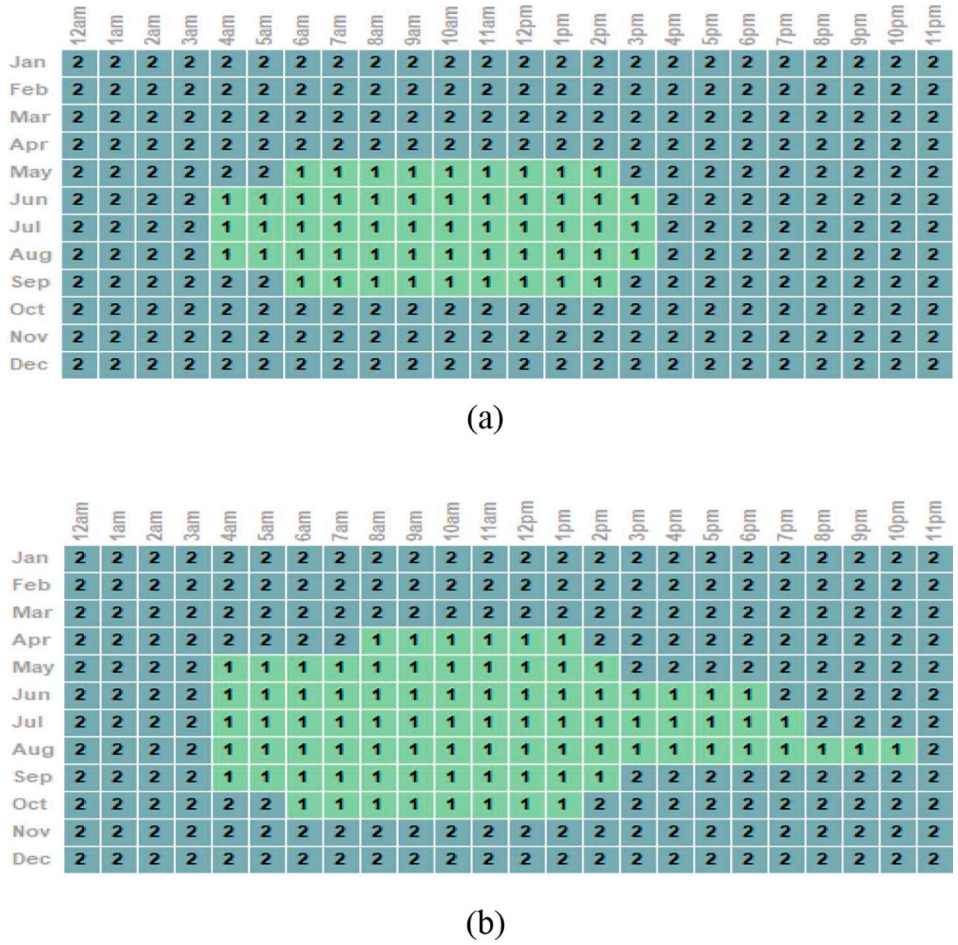

Fig. 6. The SAM hybrid condenser system control for (a) the 19% hybrid scenario and (b) the 30% scenario.

research has followed a similar methodology but with an automation performed by the LK scripting language rather than the SDK. The former permits the user of automating the SAM from the inside of the SAM simulation core and this has been chosen because of the variety of the already built in functions that it contains in addition to the pre-defined variables that the user can output and comment upon.

The LK script enabled the SAM to be operated with daily AOD values from the assembled TAY, as presented in the Section 3.1.2, in order to evaluate the effect of the temporal resolution variation of the AOD on the SPT performance. To this extent, no finer resolution than daily is considered here. As it is demonstrated in [14], an AOD resolution of up to two days is acceptable to be taken into account in arid regions such as that of Kuwait, in order to avoid any possible over/underestimation ambiguity that occurs when coarser temporal resolutions are adopted. For instance, hourly resolution is excluded here as it has not been proven to have a significant effect on the attenuation; on top of this, it comes with a significant computational penalty (in terms of time). Hence, 365 runs have been carried out for each of the 19 optimal TES-SM combinations, i.e. 6935 for each condenser type.

It is worth mentioning that the script does not change the nature of the simulation in the SAM (yearly simulation) but runs a number of simulations to the desired temporal resolution, i.e. 365. The total

outcome is basically 365 years of simulation, each of which has been run with a daily value of the AOD as obtained from the TAY. The script considers an AODi and this corresponds to day = i from the TAY and used for the SAM simulation to produce a daily outcome of an entire year (O_{year_i}). The total AEG of the script is a summation of the daily outcomes of each corresponding day i in each O_{year_i} from each simulation. For instance, day 1 of the AOD data in the TAY is automated to generate a first yearly simulation (O_{year_1}), from which the first day's energy generation is counted as the first day's outcome (O_{day_1}) of the daily AOD based script. Then the second day's energy generation of the second yearly simulation (O_{year_2}) is counted as the next daily outcome (O_{day_2}) of the daily AOD script thus forming a yearly outcome of the daily basis ($\sum O_{day\_i}$) based on the i number of the AOD values.

Results and discussion

SPT model validation

Initially, the 50 MW SPT model used in this work has been validated. The validation process has been accomplished using the data derived from Soomro et al. [84] as it is one of the few published data of a similar model and capacity. The results have been compared against the air-cooled scenario in two locations and they produce a maximum deviation of 8.8% (found in the LCOE) and this is most probably due to the differences in the weather files and the possible differences in the financial assumptions used in the simulations processes. Table 2 illustrates the comparison of both simulations.

The validation process has been limited to being performed only based on simulated data as no commercial scale SPT published data of the same capacity is available in the literature. A further step in the validation has been accomplished in order to further assess the tool's suitability. This second step of validation has been performed against the official published data of the 19.9 MW Gemasolar SPT in Spain [85] and this produced a maximum deviation of 5.1% as shown in Table 3.

In addition, the Polo model [15] has been validated in terms of the linearity with an increasing range of AOD values (Appendix A). The objectives of this work can be conducted with confidence as in despite of the different weather data, the deviation between the obtained results of this work against both commercial scale and published simulated data does not exceed 5.9% for the technical outputs (Table 4).

Preliminary performance and techno-economic assessment

By conducting a TES-SM parametric analysis, an optimal SM value is located for each TES capacity over the designated range (0–18 h) based on the lowest LCOE value and that is for each power block configuration based on different scenarios in the condenser types. The LCOE is an economic evaluation indicator that decision makers take into consideration in order to compare the plant economic performance with other similar RE, or even fossil fuel plants, as it is simply the cost of each produced kWh, and it is considered as a figure of merit for the economic viability of a plant [87].

Three power block condenser types are investigated: water-cooled, air-cooled and hybrid condensers, with the latter being examined under two different set ups: a hybridization by 30% and 19% wet cooling. It should be noted that the SAM's only set up for the hybrid condenser option is in a parallel arrangement with which the user has the ability to set up which side of the condenser is activated on an hourly schedule basis for the entire year [83]. This advantage has been used in this research based on the dry bulb temperature of the used weather file.

AEG results

In order to observe the integrated effect of the solar field size and TES capacity variation effect on the various techno-economic outputs of the plant, the SM has been varied from 1 to 4 and that is for each TES capacity from 0 h to 18 h. The variation effect is illustrated on the AEG, the water consumption and the LCOE in Figs. 7-9.

As for the AEG, the increase of the SM implies an increased quantity of the collected sun irradiance, thus more generated energy as shown in

Table 3
The validation of Gemasolar SPT.

	Our model results for Gemasolar	Reported data [85]	NREL validation [86]	Deviation (%)
Annual Energy Generation (GWh)	107.4	110	107.4	−2.4
Capacity factor (%)	70.4	74	70.4	−5.1
Cooling water requirements (m^3/year)	365,312	–	368,347	–
LCOE (¢/kWh)	18.48	–	–	–

Table 4
50 MW SPT four power block condensers types performance comparison.

	Condenser Type			
	Wet-Cooled	Air-Cooled	30% Hybrid	19% Hybrid
Annual Energy Generation (GWh)	281.4	262.6	275.4	274.8
Deviation (%)	N/A	− 6.7	− 2.1	− 2.3
Water Consumption (m^3 /a)	909,147	65,270	401,719	284,339
Deviation (%)	N/A	− 92.8	− 55.1	− 68.7

Table 2
The validation process of the SPT model against [84] in Quetta and Peshawar.

Parameters	Quetta [84]	Our model results for Quetta	Deviation (%)	Peshawar [84]	Our model results for Peshawar	Deviation (%)
Annual Energy Generation (GWh)	209.80	214.03	+ 2.1	124.09	131.12	+ 5.66
Capacity Factor (%)	53.2 %	54.3	+ 2.06	31.5	33.3	+ 5.71
Cooling water requirements (m^3/year)	38,273	39,837	+ 4.8	32,241	34,158	+ 5.94
LCOE (¢/kWh)	11.43	10.78	− 5.68	19.06	17.38	− 8.81

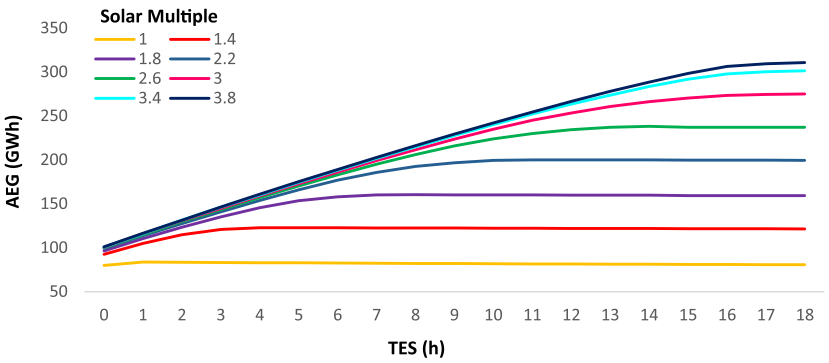

(a)

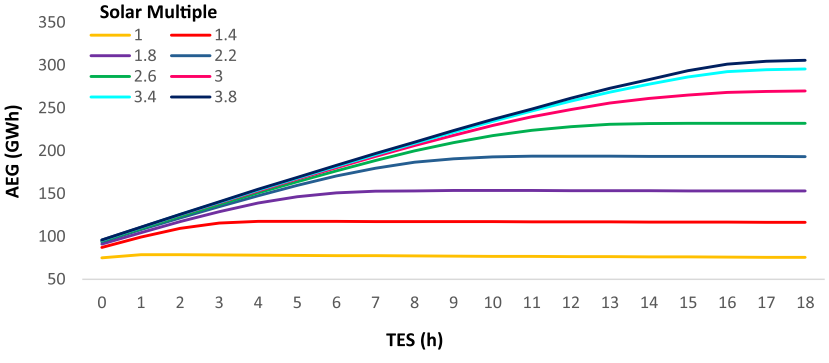

(b)

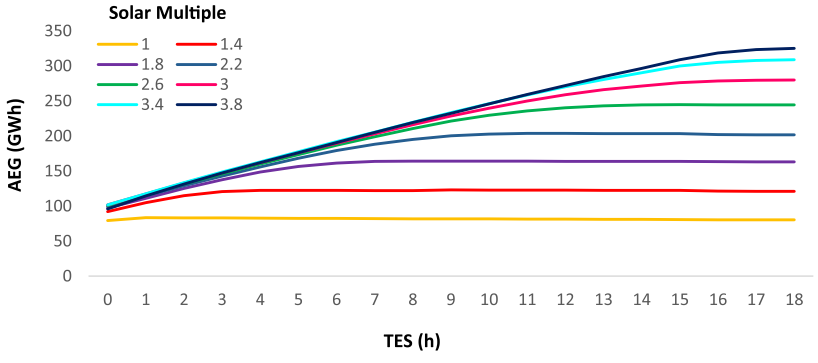

(c)

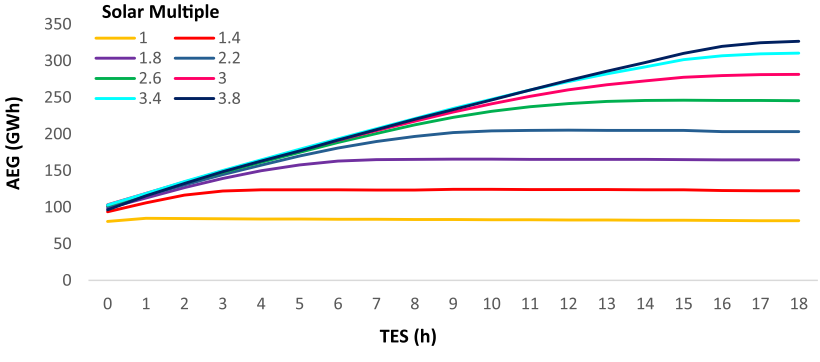

(d)

Fig. 7. The annual energy generation variation for the range of TES-SM of (a) wet-cooled condenser, (b) air-cooled condenser, (c) 19% hybrid condenser and (d) 30% hybrid condenser.

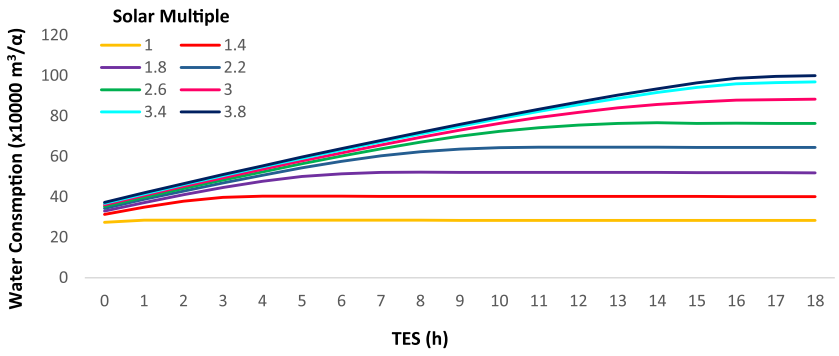

(a)

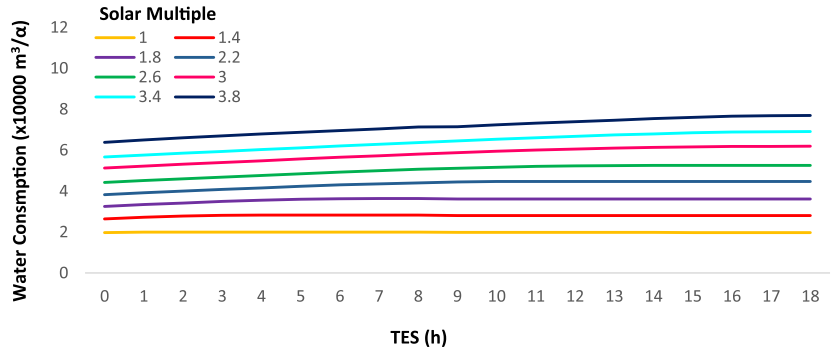

(b)

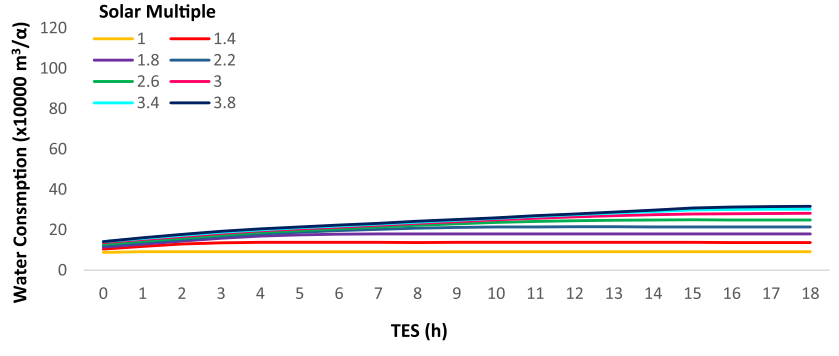

(c)

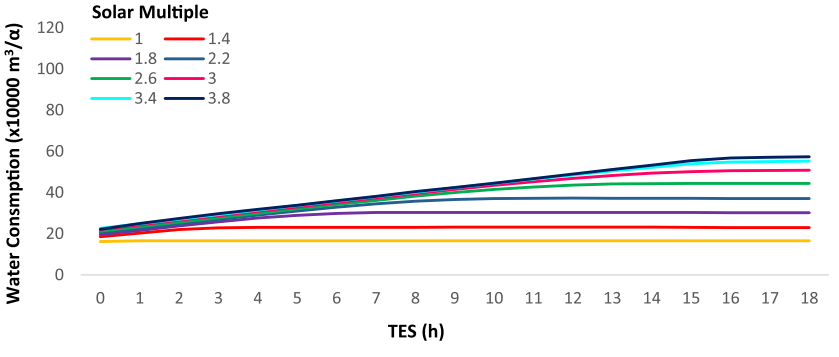

(d)

Fig. 8. The Water Consumption variation over the TES-SM ranges of (a) wet-cooled condenser, (b) air-cooled condenser, (c) 19% hybrid condenser and (d) 30% hybrid condenser.

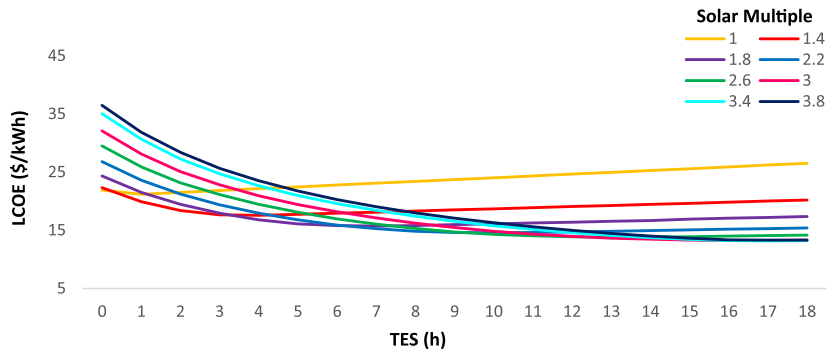

(a)

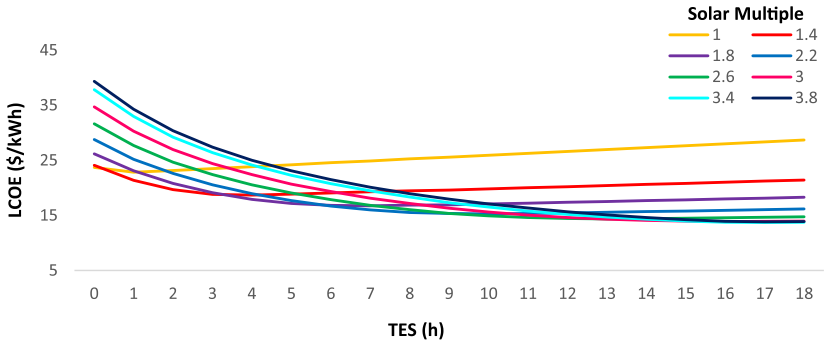

(b)

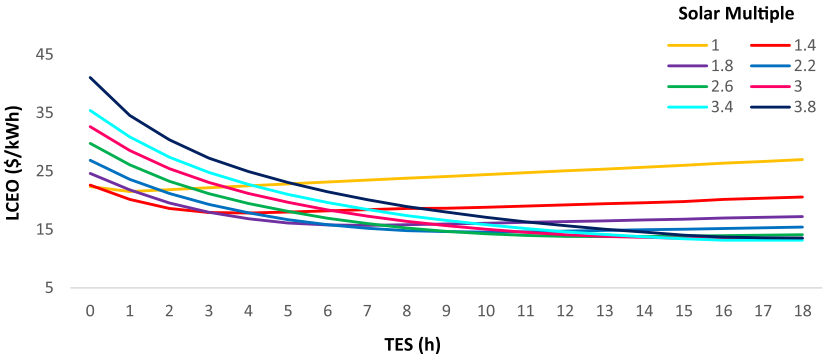

(c)

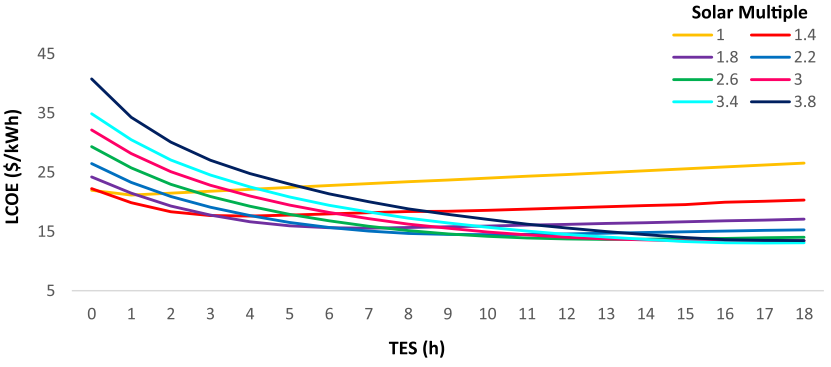

(d)

Fig. 9. The LCOE variation over the ranges of TES and SM for (a) wet-cooled condenser, (b) air-cooled condenser, (c) 19% hybrid condenser and (d) 30% hybrid condenser.

Fig. 7. The difference in the generated energy is minimal at zero storage capacity and this is only very clear as the TES increases. This is because an oversized solar field is limited in the case where no or very small TES is adopted. The proportional relation between the SM and the generated energy continues until the plant is operated at its rated capacity, after which the generated energy flattens out. It is worth noting that at higher values of SM (3.4–3.8), the generated energy is not very different. This indicates that the plant's solar field cannot be bigger as the resource irradiance will not be able to increase the generated energy accordingly. On the other hand, the Capital Expenditures (CAPEX) keeps increasing linearly as the solar field and the receiver increase in size, thus also the LCOE increases.

The variation of the TES capacity for lower values of SM has a limited effect on the AEG as seen in Fig. 7. The SM of 1 scenario actually should not be effected by the increase in the TES capacity as a SM of 1 is only supposed at best to drive the plant at its rated capacity with zero excess heat. As the SM values increases, larger are the TES capacities and this starts to have an impact on the generated energy. The effect reaches a saturation-like trend at higher capacities of the TES due to the solar irradiance limitation.

As for the cooling option, the wet-cooled condenser is supposed to easily yield the highest AEG because of the better heat rejection at the power block, however this is not exactly the case here. The SAM evaluates each configuration's ability to achieve the rated capacity of the plant (50 MW in this investigation) at each hour and hence optimizes the solar field. Since the cycle efficiency in the air-cooled scenario is lower, the air-cooled condenser scenario needs a bigger solar field for the same TES and SM compared to the wet-cooled scenario. This shrinks the gap in the AEG between both scenarios; however, the wet-cooled scenario remains with a higher AEG by 6.7% compared to the air-cooled scenario.

In addition, it is also worth mentioning that the SAM considers the hybrid condenser mainly as an air-cooled scenario as the air-cooled side of the hybrid condenser is bigger than the wet-cooled side. Thus, the solar fields of the hybrid scenarios are very similar to the air-cooled ones at the same TES and SM. Consequently, the hybrid scenarios have both the advantages of a bigger solar field and a water heat rejection in the most critical operation times of the year, thus interestingly overcomes the AEG of the air-cooled scenario by 4.6% in the 30% hybrid scenario and by 4.4% in the 19% hybrid scenario.

Water consumption results

The evolution of the water consumption is totally different as some scenarios use much less water than others. For instance, the gap in the water consumption between the different values of SM starts as being minimal and increases rapidly as the TES capacity increases in all the scenarios that involves the usage of water. Clearly, this is because at small TES capacities, the collected thermal energy of all the oversized SM values are wasted as no or too small TES is available. This means that less energy is transferred to the power block, hence there is less need of water for heat rejection. On the other hand, as the TES capacity increases, then bigger solar fields are of more use, and thus more thermal energy is transferred to the power block, which leads to more water consumption. This confirms the findings in the literature of the small percentage of the water being consumed in washing the solar field compared to that consumed at the power block. This is obvious in the air-cooled scenario shown in Fig. 8 (b) as all the values of the water consumption in this scenario are of an almost fixed value as it is only for washing the solar field reflectors and the latter are of fixed areas for a single SM value no matter how large is the TES.

However, the variation of the TES capacity has less effect on the water consumption as the latter is related to both TES and SM rather than to only one of them. For example, for smaller SM values, the water consumption is steady no matter how large the TES reaches. While for larger SM values, the water consumption appears to have a proportional relation with the TES. This is obvious in the wet-cooled condenser, as the latter is the most generating configuration due to the better heat rejection, hence the highest water consuming. In addition, this applies to the two other hybrid condenser configurations, however to a lesser extent. On the other hand, the air-cooled configuration is almost unaffected by the variation of the TES capacity. This can be explained by the fact that although as much energy may be generated but there is no usage of water in the power block, which consumes 90% of the water at such plants. The water is only for heliostats washing.

The superiority in the AEG obtained in the wet-cooled scenario over the air-cooled scenario is impaired with an elevated water consumption of 92.8% as shown in Fig. 8. This can be critical as the water transport to an arid region can sometimes be logistically very difficult. However, it cannot be entirely eliminated as the plant still needs water for other purposes, which makes the hybrid scenario an interesting consideration as it presents a trade-off between the AEG and the water consumption. To this extent, the 30% hybrid scenario resulted in a decrease of 55.1% in the water consumption compared to the wet-cooled scenario, while the 19% hybrid scenario achieved a further decrease reaching 68.7%. Here, for a fair comparison between the four different configurations, the 15 h scenario has been taken as the reference point for comparison as it yielded a similar value of SM for all configurations, i.e. 3.2.

LCOE results

Similar to the AEG, the LCOE results show a similar trend for all the scenarios as depicted in Fig. 9. The trend found in all scenarios shows that the LCOE for small values of SM begins at its minimal values and increases rapidly with the increase of the TES. Conversely, the higher values of SM begin at their highest LCOE and then decreases, reaching their minimal values at higher TES capacities. Some values in the middle of the SM range start with a decrease, however they end up by increasing again at the highest TES capacities. This trend occurs because for high values of TES and SM, the plant stores all the potential irradiance as excess heat in the TES, which is used at night and this reflects in the higher generated energy and lower LCOE. However, a further increase in the TES capacity (beyond 16–17 h for instance) is useless as the solar field size required in order to store the excess heat for 18 full load hours would be too big to be economical. This explains the rise of the LCOE after a certain point for the same SM value.

In general, lower values of LCOE are obtained in the wet-cooled scenario as the latter is of higher generation and lower capital costs compared to the air-cooled situation. This applies to the hybrid scenarios, however to a lesser extent as the lower LCOE values obtained in these two configurations are also a result of a better heat rejection, hence more energy generation in addition to the smaller air-cooled side in the hybrid configuration (compared to a fully sized air-cooled condenser).

This finding can be an indication for not having to further increase both the TES and SM. The relation between the LCOE, CAPEX, Operational Expenditures (OPEX) and the AEG is given as follows [88]:

$$LCOE = \frac{CAPEX_0 + \sum_{t=1}^{N} \frac{OPEX_t}{(1+i)t}}{\sum_{t=1}^{N} \frac{Production_t}{(1+i)t}} \quad (15)$$

where $Production_t$ is the plant production in year t (AEG). Some of the results in the literature have shown that there are more critical outputs as the LCOE increases sharply after reaching its minimum value with the continuous increase of TES and SM [16,21,89]. In this case, an increase in TES and SM is not recommended. However, the findings in this work indicates that the increase in TES and SM is left to the decision makers based on whether it is acceptable to increase the CAPEX for a minor increase in the power generation at the same/slightly higher LCOE levels. Here, the most optimal TES-SM combination has been found at the wet condenser configuration with a LCOE of 12.78 (¢/kWh) with a TES of 16 h and a SM of 3.2.

AOD temporal resolution variation effect

This section examines the difference in the SPT outputs based on the

conventional set up of the SAM compared to the recommended AOD temporal resolution in arid regions, i.e. the daily AOD. A water consumption analysis is excluded here as the SAM is limited to the output of the annual water consumption value, thus the concatenated daily outputs summation method presented in Section (3.2.5) cannot be adopted in this section.

The outputs of the preliminary parametric analysis carried in Section 4.2 has resulted in the optimal SM values for each TES capacity based on the lowest LCOE and that is for the four different condensers scenarios. For all four scenarios, all these optimal SM values are found in the range from 1.2 to 3.4. An increase in the SM values is actually an addition of new heliostats in the solar field. These new heliostats will all be placed at the outer circumference of the existing ones, which means that all newly added heliostats have an even larger slant range, thus are subject to a larger attenuation effect applied on the reflected sun irradiance that they are supposed to focus on the receiver. This effect, alongside with the larger daily values of AOD (compared to the annual averaged value, i.e. 0.3205) can theoretically mask off a considerable portion of the reflected irradiance.

AOD variation effect on the solar field and the annual energy generation

A very similar pattern can be found in all the four observed SPT configurations in terms of the effect of the daily AOD temporal resolution on: receiver incident thermal power, estimated receiver thermal power to the HTF and AEG. It has been found that the employment of the daily AOD results in a minor difference in the thermal power from the solar field (this does not exceed 1.1% and this is shown in Appendix B) in all the SM values over the designated range. Despite the gradual increase in the slant range, as a result of increasing the SM value, no substantial increase in the deviation of the thermal power from the solar field has been found. A linearity has been found in the latter range as the deviation increases gradually, however, close to the conventional solar field thermal power based on the annually averaged AOD value (0.3205). It has been found that no matter how large is the increase in the slant range for this specific plant's capacity in this case study location, the AEG is not substantially affected, which is most probably due to the other factors in the equation being not very important, e.g. the AOD intensity and/or AOD temporal variability.

Despite the limited effect of the daily AOD temporal resolution adoption, it would still be very critical in the case when such an investigation has not been done in such a region. That is why a comparison between both the annually averaged and daily AOD temporal resolutions has been carried out against the no aerosols scenario. Fig. 10 (a) illustrates the latter effect uniquely on the daily energy generation for the optimal (lowest LCOE) wet-cooled configuration of 16 h at SM of 3.2. In addition, it is also worth mentioning that the authors considered that the large TES capacity might play a role in the mitigation of the temporal resolution's variation effect, thus a similar examination has been carried at the optimal TES-SM combination with a TES of 0 h, as shown in Fig. 10 (b).

In the 0 h TES scenario, the daily AOD temporal resolution resulted in a decrease of 0.6% in the AEG compared to the annually averaged

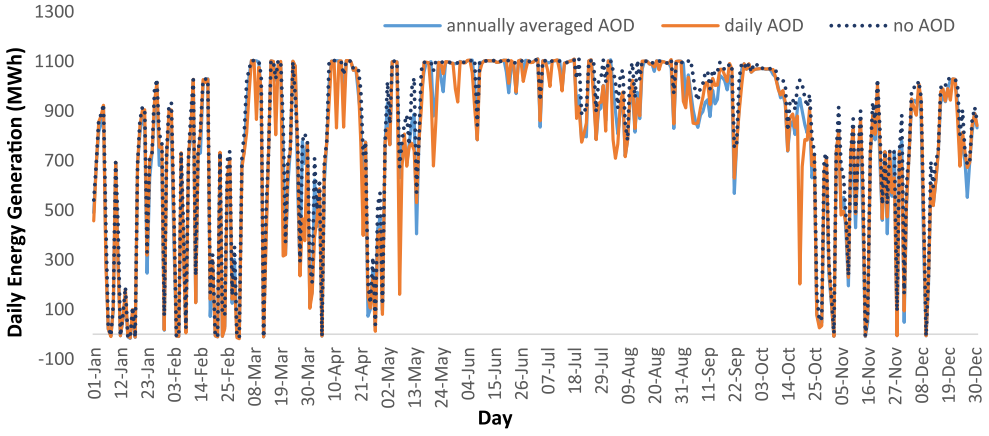

(a)

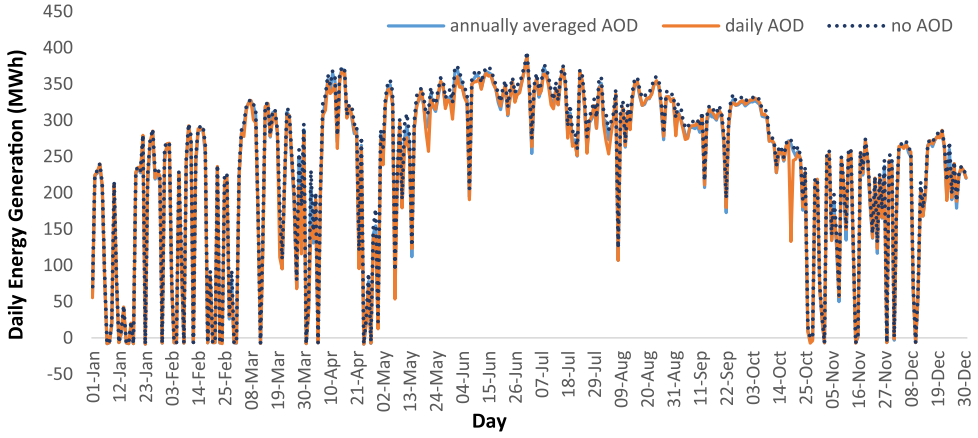

(b)

Fig. 10. The AOD temporal resolution variation effect on the daily energy generation for (a) 16 h of TES and (b) 0 h of TES.

AOD (0.3205) and a decrease of 3.7% compared to the no aerosols scenario. As for the 16 h TES scenario, the daily AOD resolution yielded a decrease of 1% compared to the annually averaged case, while a decrease of 6.7% has been obtained between the former and the no aerosols scenario. Clearly, it is seen that having a bigger solar field results in an elevated attenuation extinction, even in the case of having a large TES capacity such as the case examined here, i.e. 16 h. Larger plants capacities, which have larger solar fields, will most probably have an amplified effect of aerosols even in the case when large TES are adopted.

Another very important finding is that despite the limited percentage of AEG decrease after examining the plant under the daily AOD resolution, the plant still has a considerable percentage of deviation in the daily energy generation on specific days as the solar field is affected substantially on some aerosols peak days. Fig. 11 illustrates how the solar fields of the two configurations presented in Fig. 10 are affected on specific days based on different aerosols scenarios.

Due to some abnormally elevated AOD daily values, which are most likely caused by dust storms, the daily energy generation on some days of the year witnesses a more considerable deviation. Depending on the TES-SM scenario, the daily energy generation of an aerosols dense day (18th of October on a 16 h and SM 3.2 wet-cooled configuration for instance) can be overestimated by 77.8% as the annually averaged AOD simulation results in 912.1 kW, while based on the daily AOD, the same simulation only gives 202.1 kW. This signifies how the daily AOD case can give a better estimation of the daily generated energy, thus better estimation of the SPT' daily energy delivery commitment to the grid. This finding is very important for the grid control purposes as it can be used for the plant daily energy generation forecast work.

AOD effect on the LCOE

The deviation of the solar field thermal output due to the adoption of different temporal resolutions translates into a deviation in the absorbed thermal energy to the HTF and finally to a deviation also in the AEG as seen in the last section. This will of course have an effect on the LCOE as the latter is directly related to the AEG, as shown in equation (15). However, since the deviation in the AEG has been insignificant, the same trend is expected for the LCOE. Each optimal SM value is located for each TES capacity based on the lowest value of the LCOE and this presented in Table 5, which initially illustrates the evolution of the AEG, capacity factor and the LCOE based on the annually averaged AOD value (0.3205), and then compares these outputs against those of the no aerosols and daily AOD scenarios.

A maximum increase of 6.8% has been observed in the LCOE when the daily AOD is adopted compared to the no-aerosols scenario. This in turn qualifies the SPT technology to be suitable in this specific location and the 50 MW plant capacity. The aerosols are one of the most important factors that threats the success of such a technology and the estimated small effect on both the AEG and the LCOE suggest that there exist good prospects for potential future applications. Further, the techno-economic outputs of multiple commercial and simulated CSP plants of the same capacity have been compared against the results of the daily aerosols scenario of this work as shown in Table 6.

Despite the deviation imposed by the application of the daily AOD resolution on the AEG and the LCOE, the 50 MW SPT model simulated in this work shows some very promising and competitive results when compared with other similar operational and simulated CSP plants of the same plant capacity. In addition, it is very encouraging that the lowest LCOE of these TES-SM ranges in all aerosols scenarios is lower than the average actual cost of electricity in the conventional fossil fuel plants in Kuwait, i.e. 14 ¢/kWh [95,96]. This is a sign of the reliability of the SPT, as the effect of the aerosols on the AEG appears to be relatively low. In addition, the daily aerosols adoption emerged as a realistic methodology in such regions and this reduces the chance of inaccuracies in the techno-economic assessments and gives better estimation of the annually as well as the daily energy generation. This finding signifies the importance of the normalization of this process in the prefeasibility stage for such a technology, especially because other similar arid regions have been proven to have an amplified effect of aerosols on the solar field while having close annual averaged AOD values to the one in this study. Further, it should be borne in mind that for bigger capacities consisting of bigger solar field of the same technology and in the same location might result in bigger deviations in the AEG when daily aerosols values are adopted. This has been clearly seen in the daily AOD adoption when applied on two different TES-SM scenarios, i.e. the first with no TES and a small solar field, while the second is with a large TES (16 h) and a large solar field. It is very interesting to note that the deviation in the AEG of the larger solar field scenario is affected more than that of the smaller solar field and that is despite having a large TES that should have mitigated the attenuation effect.

Conclusion and future work

A new multiple temporal resolutions aerosols techno-economic assessment of a SPT in arid regions has been proposed in this paper. This has been based on an arid remote region in Kuwait, where the irradiation levels are elevated, however these may be heavily attenuated by the frequent sand storms. Thus, we have quantified the aerosols effect and included it as a probable factor in the attenuation of the main key design parameter in such technology, i.e. the DNI. Likewise, the DNI is more accurately measured and only then, the parametric analysis of the TES-SM sizing strategy has been implemented. Conversely, in the case that the aerosols are excluded from the assessment, and this is usually the situation in the literature, the DNI, which is the main design parameter of the technology is often amplified and eventually this leads to probable incorrect evaluations of the DNI resource. Thus, this leads to an inappropriate solar field size. A too big/small solar field size translates into what appears to be a higher/lower capital cost, which drives the LCOE higher/lower than it is actually. Often, this leads to wrong, or misleading estimations for the decision makers.

For this reason, the most reliable, yet short-term ground measurement of aerosols data has been acquired in order to site adapt the longer term MERRA-2 reanalysis data. The site adaptation, which has been realized by the employment of a quantile mapping technique, has managed to minimally reduce the bias that exists between the short and long-term sets of data. The bias corrected new long-term data has been employed in the Finkelstein-Schafer statistics in order to assemble a TAY. As a result, a year of the annually averaged AOD values from the site adapted TAY has been found to be 0.3205 and this has been integrated into the solar field attenuation extinction function in the SAM simulation tool with the assistance of the Polo model [15].

Further, the same parametric analysis has been performed but with four different cooling options: wet, dry and two hybrid scenarios in a trial to optimize the SPT water consumption, as it is firstly considered as another threat to the feasibility of CSP in arid regions, and secondly, it is found that the cooling type contributes to the amount of energy generated, which is only clearly observed when there is a variation in both the TES and SM. In addition, the cooling type variation comes with an impact on both the LCOE, and thus it has to be also assessed and presented. The aerosols are just an attenuation factor of the DNI which, along with the cooling type, are directly related to the energy generation; the DNI is a thermal energy input in the solar field, while the cooling type is an efficiency enhancement factor in the power block.

Two dry bulb temperatures of reference have been observed and these have been used in order to optimize the hybrid scenarios set ups, namely 32 °C and 37 °C. This resulted in the first hybrid set up being with a 30% wet side activation and the other with only 19% wet side activation. Both hybrid set-ups have managed to reduce drastically the water consumption by 55.1 and 68.7%, respectively. In addition, both hybrid set ups surpassed the AEG of the air-cooled scenario by 4.6 and 4.4%, respectively. Due to the minor improvement offered by the 30% hybrid scenario in the AEG compared to that of the 19% scenario, in

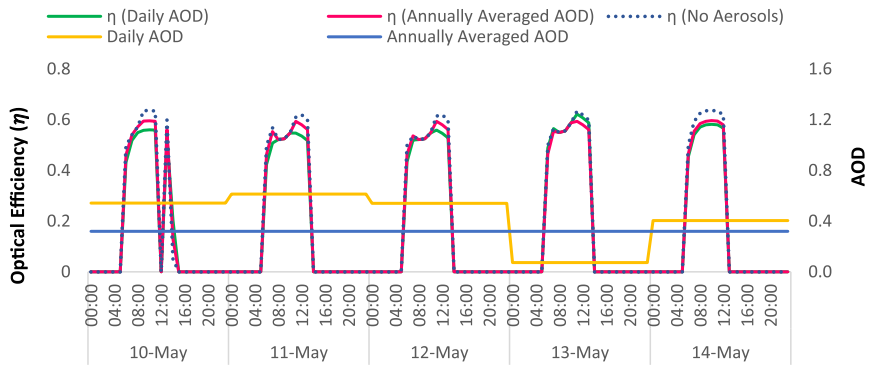

(a)

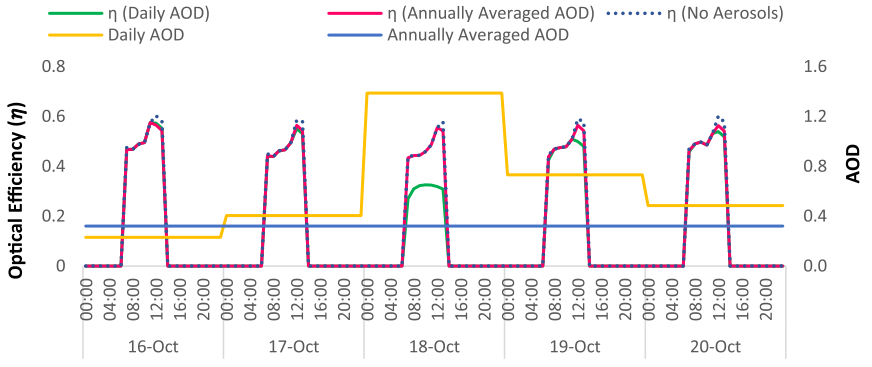

(b)

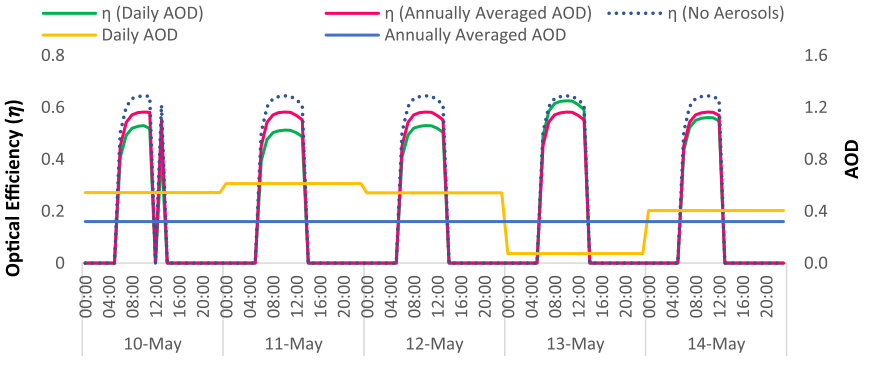

(c)

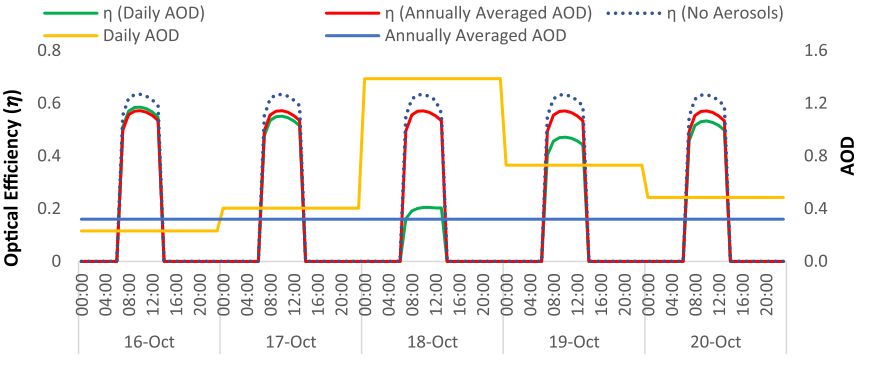

(d)

Fig. 11. The solar field optical efficiency based on different scenarios for (a) and (b) the 0 h TES and the 16 h TES in (c) and (d).

Table 5
The 50 MW SPT optimal TES-SM outputs based on the annually averaged AOD and compared to different aerosols temporal resolutions: No aerosols[1] and daily AOD[2].

Condenser Type	Wet				Dry			
TES (h)	Optimal SM (-)	LCOE (¢/kWh)	AEG (GWh)	CF (%)	Optimal SM (-)	LCOE (¢/kWh)	AEG (GWh)	CF (%)
0	1.2	20.49[1] 21.14 21.24[2]	90.6[1] 87.7 87.2[2]	22.3	1.2	23.15[1] 23.94 24.07[2]	80.7[1] 77.9 77.5[2]	19.8
3	1.6	16.45[1] 17.03 17.15[2]	135.2[1] 130.5 129.4[2]	33.1	1.6	18.32[1] 18.97 19.09[2]	122.5[1] 118.2 117.3[2]	30
6	2	14.57[1] 15.18 15.29[2]	177.1[1] 169.8 168.2[2]	43.1	2	16.2[1] 16.9 17[2]	162.4[1] 155.4 154.3[2]	39.4
9	2.4	13.49[1] 14.13 14.2[2]	218.3[1] 208.2 206.7[2]	52.8	2.2	14.75[1] 15.72 15.81[2]	192.7[1] 180.6 179.2[2]	45.8
12	2.8	12.72[1] 13.36 13.45[2]	257.8[1] 244.9 242.7[2]	62.1	2.8	14[1] 14.75 14.85[2]	239.6[1] 226.9 224.9[2]	57.6
15	3.2	12.22[1] 12.91 13[2]	297.8[1] 281.4 278.7[2]	71.4	3.2	13.41[1] 14.2 14.3[2]	278.5[1] 262.6 260.2[2]	66.6
18	3.4	12.19[1] 12.86 12.96[2]	318.2[1] 301.1 298.1[2]	76.4	3.2	13.23[1] 14.08 14.2[2]	285.9[1] 268.2 265.2[2]	68

Condenser Type	30% Hybrid				19% Hybrid			
TES (h)	Optimal SM (-)	LCOE (¢/kWh)	AEG (GWh)	CF (%)	Optimal SM (-)	LCOE (¢/kWh)	AEG (GWh)	CF (%)
0	1.2	21.56[1] 22.3 22.42[2]	87.1[1] 84.5 83.6[2]	21.3	1.2	21.68[1] 22.43 22.55[2]	86.6[1] 83.7 83.1[2]	21.2
3	1.6	17.17[1] 17.78 17.89[2]	131.2[1] 126.6 125.6[2]	32	1.6	17.35[1] 17.97 18.08[2]	130.3[1] 125.7 124.8[2]	31.9
6	2	15.2[1] 15.87 15.96[2]	172.5[1] 164.9 163.8[2]	41.8	2	15.3[1] 15.97 16.06[2]	171.5[1] 164.1 162.9[2]	41.6
9	2.4	14.08[1] 14.76 14.85[2]	213.1[1] 203.1 201.5[2]	51.3	2.4	14.17[1] 14.86 14.95[2]	211.8[1] 201.8 200.2[2]	51.2
12	2.8	13.35[1] 14.03 14.13[2]	251.8[1] 239.2 236.9[2]	60.5	2.8	13.44[1] 14.14 14.24[2]	251.3[1] 238.6 236.3[2]	60.5
15	3.2	12.82[1] 13.54 13.64[2]	291.2[1] 275.2 272.5[2]	69.9	3.2	12.83[1] 13.56 13.65[2]	290.9[1] 274.8 272.2[2]	69.7
18	3.2	12.77[1] 13.47 13.58[2]	310.4[1] 293.7 290.6[2]	71.7	3.4	12.8[1] 13.5 13.6[2]	308.8[1] 292.2 289.3[2]	74.1

[1] No Aerosols.
[2] Daily AOD.

addition to the much larger water saving that the latter offers, the 19% hybrid set up can be suggested as an appropriate good candidate in the case where the wet-cooled condenser is not an option.

Consequently, a parametric analysis of the SPT model based on the annually averaged AOD value has been performed by varying the TES capacity from 0 h to 18 h and the SM value from 1 to 4, aiming to identify the TES-SM combination that results in the lowest LCOE. The lowest LCOE among all the configurations based on the annually averaged AOD has been found to be 12.78 ¢/kWh in the wet-cooled configuration and that is at a TES of 16 h and a SM of 3.2, while a LCOE of 12.06 ¢/kWh has been found for the no aerosols scenario. Further, since aerosols are characterized by their high spatiotemporal variability, the LCOE of each optimal TES-SM combination of the parametric analysis has been observed based on the daily AOD resolution and found to be 12.87 ¢/kWh which is 6.7% from the no aerosols scenario and 0.7% from the annually averaged AOD scenario.

Table 6
Comparison of the modelled results in this work with both commercial and modelled 50 MW CSP plants.

Project Name/ Publication	Location	Site Annual DNI (kWh/m^2)	CSP Type	Condenser Type	TES capacity (h)	Capacity Factor (%)	LCOE (¢/kWh)	AEG (GWh)
Termesol 50 [90]	Spain	2097	PTC	Wet Cooling	7.5	40	–	175
Andasol 3 [91]	Spain	2200	PTC	Wet Cooling	7.5	40	–	175
La Africana [91]	Spain	1950	PTC	Wet Cooling	7.5	39	–	170
Hirbodi et al. [21]	Iran	–	PTC	Wet Cooling	15	73.9	14.6	320.4
				Air Cooling	15	73.5	15.2	318.6
			SPT	Wet Cooling	15	86.6	12.3	375.5
				Air Cooling	15	85.7	12.6	371.5
Sultan et al. [16]	Kuwait	1857	PTC	Air Cooling	16	60.4	15.07	238.2
Dersch et al. [92]	Spain	2111	SPT	–	7.5	40	–	161.1
Li et al. [93]	China	–	SPT	–	10	–	–	208.2
Chen et al. [26]	China	2752	SPT	–	15	–	13.77	361.1
Ouali and Richert [94]	Morocco	1989.9	SPT	–	7	–	–	159.07
Mihoub et al. [19]	Algeria	2008.4	SPT	–	8	45	23.57	193
Soomro et al. [84]	Pakistan	1992.9	SPT	Wet cooling	12	57.6	10.98	233.23
This work	Kuwait	2241	SPT	Wet Cooling	16	73.1	12.87	285.2
				Air Cooling	16	67.9	14.1	264.9
				30% Hybrid	17	74.2	13.48	289.9
				19% Hybrid	17	73.9	13.56	288.6

The variation of the slant range through solar field's optimization has been performed in the current work over the SM range of 1–4 along with the variation of TES capacity and this resulted in different aerosols effect on the solar field, and thus different reduction percentages of the AEG ranging from 0.6 – 6.7% (for the wet-cooled scenario). This signifies how sensitive the AEG is to the solar field size with one specific location's aerosols levels despite the gradual contribution of the TES in the compensation of the reduced AEG along with the increasing size of the solar field. The maximum obtained reduction of the current work is considered as low/intermediate compared to the results found in [28] (20 %) which examined different aerosols density levels of multiple locations based on only two fixed configurations.

While the work of Polo et al. [28] has confirmed a non-negligible effect of the aerosols on the reflected irradiance of the SPT solar field, the current work made use of similar tools to first evaluate the aerosols effects and then presented a general SPT sizing strategy methodology with which the user can define the appropriate TES-SM configuration given the effect of aerosols on each solar field size and the role of TES in the compensation of the reduced AEG (due to the aerosols attenuation). The methodology also detailed how the LCOE has been affected by both the reduction of the AEG and the variation of the capital costs (by varying the TES).

Although being able to reveal how sensitive the solar field is to the adoption of aerosols over a wide range of TES-SM for a 50 MW SPT, higher SPT plant capacities are expected to have higher reductions in the AEG when aerosols effects are included, as they consist of larger slant ranges (due to the addition of the new heliostats at the outer circumference of the already existing heliostats). Therefore, as future research, the examination of higher plant capacities is highly recommended. In addition, the suspended aerosols will not only have an effect on the irradiance in the solar field, but will also participate in the soiling phenomena. These are common in arid regions and have been reported [97,98] with non-negligible effects on both solar and non-solar renewable energy applications in the same case study location as in this work. Thus, further work which relates soiling to the metrological parameters (including aerosols) is of importance and can assist in operation strategies planning, e.g. reflectors washing, water saving optimization, etc.

CRediT authorship contribution statement

Mohammed S. Alfailakawi: Conceptualization, Investigation, Methodology, Software, Validation, Formal analysis, Writing – original draft. **Stavros Michailos:** Investigation, Methodology, Software, Validation, Writing – review & editing. **Derek B. Ingham:** Resources, Writing – review & editing, Supervision, Project administration. **Kevin J. Hughes:** Resources, Supervision, Project administration. **Lin Ma:** Resources, Supervision, Project administration. **Mohamed Pourkashanian:** Resources, Supervision, Project administration.

Declaration of Competing Interest

The authors declare that they have no known competing financial interests or personal relationships that could have appeared to influence the work reported in this paper.

Acknowledgements

The authors would like to acknowledge the Kuwait Ministry of Defense for their valuable financial support. Also, thanks to Dr. Majed AL-Rasheedi from the KISR for making the weather data available for this research.

Appendix A. Supplementary data

Supplementary data to this article can be found online at https://doi.org/10.1016/j.seta.2022.102324.

References

[1] Burgaleta JI, Arias S, Ramirez D. Gemasolar, the first tower thermosolar commercial plant with molten salt storage. Solarpaces 2011:1–8.
[2] Dunn RI, Hearps PJ, Wright MN. Molten-salt power towers: Newly commercial concentrating solar storage. Proc IEEE 2012;100:504–15. https://doi.org/10.1109/JPROC.2011.2163739.
[3] Balghouthi M, Trabelsi SE, Ben AM, Ali ABH, Guizani A. Potential of concentrating solar power (CSP) technology in Tunisia and the possibility of interconnection with Europe. Renew Sustain Energy Rev 2016;56:1227–48. https://doi.org/10.1016/j.rser.2015.12.052.
[4] Shahabuddin M, Alim MA, Alam T, Mofijur M, Ahmed SF, Perkins G. A critical review on the development and challenges of concentrated solar power technologies. Sustain Energy Technol Assessments 2021;47:101434. https://doi.org/10.1016/j.seta.2021.101434.
[5] Islam MT, Huda N, Abdullah AB, Saidur R. A comprehensive review of state-of-the-art concentrating solar power (CSP) technologies: Current status and research trends. Renew Sustain Energy Rev 2018;91:987–1018. https://doi.org/10.1016/j.rser.2018.04.097.

[6] Zhang HL, Baeyens J, Degrève J, Cacères G. Concentrated solar power plants: Review and design methodology. Renew Sustain Energy Rev 2013;22:466–81. https://doi.org/10.1016/j.rser.2013.01.032.
[7] Siva Reddy V, Kaushik SC, Ranjan KR, Tyagi SK. State-of-the-art of solar thermal power plants - A review. Renew Sustain Energy Rev 2013;27:258–73. https://doi.org/10.1016/j.rser.2013.06.037.
[8] Trieb F, Schillings C, O'Sullivan M, Pregger T, Hoyer-Klick C. Global Potential of Concentrating Solar Power. Conf. Proc., Berlin: 2009, p. 1–11.
[9] Khalil SA, Shaffie AM. Attenuation of the solar energy by aerosol particles: A review and case study. Renew Sustain Energy Rev 2016;54:363–75. https://doi.org/10.1016/j.rser.2015.09.085.
[10] Gueymard CA. Uncertainties in modeled direct irradiance around the sahara as affected by aerosols: Are current datasets of bankable quality. J Sol Energy Eng Trans ASME 2011;133:1–13. https://doi.org/10.1115/1.4004386.
[11] Gueymard CA. Impact of on-site atmospheric water vapor estimation methods on the accuracy of local solar irradiance predictions. Sol Energy 2014;101:74–82. https://doi.org/10.1016/j.solener.2013.12.027.
[12] Gueymard CA. Temporal variability in direct and global irradiance at various time scales as affected by aerosols. Sol Energy 2012;86:3544–53. https://doi.org/10.1016/j.solener.2012.01.013.
[13] Gueymard CA. Visibility, aerosol conditions, and irradiance attenuation close to the ground-Comments on "Solar radiation attenuation in solar tower plants" by J. Ballestrin and A. Marzo, Solar Energy (2012). Sol Energy 2012;86:1667–8. Doi: 10.1016/j.solener.2011.12.027.
[14] Ruiz-Arias JA, Gueymard CA, Santos-Alamillos FJ, Pozo-Vázquez D. Worldwide impact of aerosol's time scale on the predicted long-term concentrating solar power potential. Sci Rep 2016;6. https://doi.org/10.1038/srep30546.
[15] Polo J, Ballestrín J, Carra E. Sensitivity study for modelling atmospheric attenuation of solar radiation with radiative transfer models and the impact in solar tower plant production. Sol Energy 2016;134:219–27. https://doi.org/10.1016/j.solener.2016.04.050.
[16] Sultan AJ, Hughes KJ, Ingham DB, Ma L, Pourkashanian M. Techno-economic competitiveness of 50 MW concentrating solar power plants for electricity generation under Kuwait climatic conditions. Renew Sustain Energy Rev 2020;134. https://doi.org/10.1016/j.rser.2020.110342.
[17] Rouibah A, Benazzouz D, Kouider R, Al-Kassir A, García-Sanz-Calcedo J, Maghzili K. Solar tower power plants of molten salt external receivers in Algeria: Analysis of direct normal irradiation on performance. Appl Sci 2018;8. https://doi.org/10.3390/app8081221.
[18] Boudaoud S, Khellaf A, Mohammedi K, Behar O. Thermal performance prediction and sensitivity analysis for future deployment of molten salt cavity receiver solar power plants in Algeria. Energy Convers Manag 2015;89:655–64. https://doi.org/10.1016/j.enconman.2014.10.033.
[19] Mihoub S, Chermiti A, Beltagy H. Methodology of determining the optimum performances of future concentrating solar thermal power plants in Algeria. Energy 2017;122:801–10. https://doi.org/10.1016/j.energy.2016.12.056.
[20] Murat CH. A Comparison of Solar Power Systems (CSP): Solar Tower (ST) Systems versus Parabolic Trough (PT) Systems. Am J Energy Eng 2015;3:29. https://doi.org/10.11648/j.ajee.20150303.11.
[21] Hirbodi K, Enjavi-Arsanjani M, Yaghoubi M. Techno-economic assessment and environmental impact of concentrating solar power plants in Iran. Renew Sustain Energy Rev 2020;120. https://doi.org/10.1016/j.rser.2019.109642.
[22] Agyekum EB, Velkin VI. Optimization and techno-economic assessment of concentrated solar power (CSP) in South-Western Africa: A case study on Ghana. Sustain Energy Technol Assessments 2020;40:100763. https://doi.org/10.1016/j.seta.2020.100763.
[23] Izquierdo S, Montañs C, Dopazo C, Fueyo N. Analysis of CSP plants for the definition of energy policies: The influence on electricity cost of solar multiples, capacity factors and energy storage. Energy Policy 2010;38:6215–21. https://doi.org/10.1016/j.enpol.2010.06.009.
[24] Coelho B, Varga S, Oliveira A, Mendes A. Optimization of an atmospheric air volumetric central receiver system: Impact of solar multiple, storage capacity and control strategy. Renew Energy 2014;63:392–401. https://doi.org/10.1016/j.renene.2013.09.026.
[25] Casati E, Casella F, Colonna P. Design of CSP plants with optimally operated thermal storage. Sol Energy 2015;116:371–87. https://doi.org/10.1016/j.solener.2015.03.048.
[26] Chen R, Rao Z, Liao S. Determination of key parameters for sizing the heliostat field and thermal energy storage in solar tower power plants. Energy Convers Manag 2018;177:385–94. https://doi.org/10.1016/j.enconman.2018.09.065.
[27] Hanrieder N, Wilbert S, Mancera-Guevara D, Buck R, Giuliano S, Pitz-Paal R. Atmospheric extinction in solar tower plants – A review. Sol Energy 2017;152:193–207. https://doi.org/10.1016/j.solener.2017.01.013.
[28] Polo J, Ballestrín J, Alonso-Montesinos J, López-Rodriguez G, Barbero J, Carra E, et al. Analysis of solar tower plant performance influenced by atmospheric attenuation at different temporal resolutions related to aerosol optical depth. Sol Energy 2017;157:803–10. https://doi.org/10.1016/j.solener.2017.09.003.
[29] Carra E, Ballestrín J, Polo J, Barbero J, Fernández-Reche J. Atmospheric extinction levels of solar radiation at Plataforma Solar de Almería. Application to solar thermal electric plants. Energy 2018;145:400–7. https://doi.org/10.1016/j.energy.2017.12.111.
[30] Muñoz J, Martínez-Val JM, Abbas R, Abánades A. Dry cooling with night cool storage to enhance solar power plants performance in extreme conditions areas. Appl Energy 2012;92:429–36. https://doi.org/10.1016/j.apenergy.2011.11.030.
[31] Marugán-Cruz C, Sánchez-Delgado S, Gómez-Hernández J, Santana D. Towards zero water consumption in solar tower power plants. Appl Therm Eng 2020;178:115505. https://doi.org/10.1016/j.applthermaleng.2020.115505.
[32] U.S. Department of Energy. Concentrating solar power commercial application study: Reducing water consumption of concentrating solar power electricity generation. vol. 2001; 2010.
[33] Poullikkas A, Hadjipaschalis I, Kourtis G. A comparative overview of wet and dry cooling systems for Rankine cycle based CSP plants. Trends Heat Mass Transf 2013;13:27–50.
[34] Wagner MJ, Kutscher C. THE IMPACT OF HYBRID WET / DRY COOLING ON CONCENTRATING SOLAR POWER PLANT PERFORMANCE. Proc ASME 2010 4th Int Conf Energy Sustain 2010:1–8. Doi: 10.1115/es2010-90442.
[35] Duvenhage DF, Brent AC, Stafford WHL. The need to strategically manage CSP fleet development and water resources: A structured review and way forward. Renew Energy 2019;132:813–25. https://doi.org/10.1016/j.renene.2018.08.033.
[36] Rutberg MJ (Michael J. Modeling water use at thermoelectric power plants; 2012:77.
[37] Qoaider L, Liqreina A. Optimization of dry cooled parabolic trough (CSP) plants for the desert regions of the Middle East and North Africa (MENA). Sol Energy 2015;122:976–85. https://doi.org/10.1016/j.solener.2015.10.021.
[38] Ben FMS, Abderafi S. Water consumption analysis of Moroccan concentrating solar power station. Sol Energy 2018;172:146–51. https://doi.org/10.1016/j.solener.2018.06.003.
[39] Blanco-Marigorta AM, Victoria Sanchez-Henríquez M, Peña-Quintana JA. Exergetic comparison of two different cooling technologies for the power cycle of a thermal power plant. Energy 2011;36:1966–72. https://doi.org/10.1016/j.energy.2010.09.033.
[40] Yilmazoglu MZ. Effects of the selection of heat transfer fluid and condenser type on the performance of a solar thermal power plant with technoeconomic approach. Energy Convers Manag 2016;111:271–8. https://doi.org/10.1016/j.enconman.2015.12.068.
[41] Aly A, Bernardos A, Fernandez-Peruchena CM, Jensen SS, Pedersen AB. Is Concentrated Solar Power (CSP) a feasible option for Sub-Saharan Africa?: Investigating the techno-economic feasibility of CSP in Tanzania. Renew Energy 2019;135:1224–40. https://doi.org/10.1016/j.renene.2018.09.065.
[42] Asfand F, Palenzuela P, Roca L, Caron A, Lemarié CA, Gillard J, et al. Thermodynamic performance and water consumption of hybrid cooling system configurations for concentrated solar power plants. Sustain 2020;12. https://doi.org/10.3390/su12114739.
[43] Atalay Y, Biermann F, Kalfagianni A. Adoption of renewable energy technologies in oil-rich countries: Explaining policy variation in the Gulf Cooperation Council states. Renew Energy 2016;85:206–14. https://doi.org/10.1016/j.renene.2015.06.045.
[44] Gueymard CA, Al-Rasheedi M, IsA, Hussain T. Long-Term variability of aerosol optical depth, dust episodes, and direct normal irradiance over Kuwait for CSP Applications. ISES Sol World Congr 2017 - IEA SHC Int Conf Sol Heat Cool Build Ind 2017, Proc 2017:75–84. Doi: 10.18086/swc.2017.04.04.
[45] Binamer AO. Al-Abdaliya integrated solar combined cycle power plant: Case study of Kuwait, part I. Renew Energy 2019;131:923–37. https://doi.org/10.1016/j.renene.2018.07.076.
[46] Al-Hajraf S. Feasibility Study of Renewable Energy Technologies for Power Generation in the State of Kuwait; 2010.
[47] Al-Rasheedi M, Gueymard C, Al-Hajraf S, IsA. Solar Resource Assessment over Kuwait: Validation of Satellite-derived Data and Reanalysis Modeling; 2015:1–10. Doi: 10.18086/eurosun.2014.08.01.
[48] Alshawaf M, Poudineh R, Alhajeri NS. Solar PV in Kuwait: The effect of ambient temperature and sandstorms on output variability and uncertainty. Renew Sustain Energy Rev 2020;134:110346. https://doi.org/10.1016/j.rser.2020.110346.
[49] Lude S, Fluri TP, Alhajraf S, Jülch V, Kühn P, Marful A, et al. Optimization of the Technology Mix for the Shagaya 2 GW Renewable Energy Park in Kuwait. Energy Procedia 2015;69:1633–42. https://doi.org/10.1016/j.egypro.2015.03.120.
[50] Marful AB. MASTER PLANNING TO HARNESS THE SUN AND WIND ENERGY: The Case of Shagaya Renewable Energy Master Plan Project, Kuwait. MIPALCON 2014 Clim. Chang. – A Glob. Challenge. Contrib. Infrastruct. Plan., Stuttgart: 2016, p. 105–15.
[51] Polo J, Wilbert S, Ruiz-arias JA, Meyer R, Gueymard C, Su M, et al. ScienceDirect Preliminary survey on site-adaptation techniques for satellite-derived and reanalysis solar radiation datasets 2016; 132:25–37. Doi: 10.1016/j.solener.2016.03.001.
[52] Cebecauer T, Suri M. Site-adaptation of satellite-based DNI and GHI time series: Overview and SolarGIS approach. AIP Conf Proc 2016;1734. https://doi.org/10.1063/1.4949234.
[53] Holben BN, Eck TF, Slutsker I, Tanré D, Buis JP, Setzer A, et al. AERONET - A federated instrument network and data archive for aerosol characterization. Remote Sens Environ 1998;66:1–16. https://doi.org/10.1016/S0034-4257(98)00031-5.
[54] NASA. The Modern-Era Retrospective analysis for Research and Applications Version 2 (MERRA-2) n.d. https://gmao.gsfc.nasa.gov/reanalysis/%0AMERRA-2/ (accessed November 20, 2020).
[55] Feigenwinter I, Kotlarski S, Casanueva A, Fischer A, Schwierz C, Liniger MA. Exploring quantile mapping as a tool to produce user tailored climate scenarios for Switzerland. Tech Rep MeteoSwiss 2018.
[56] Fernández-Peruchena CM, Polo J, Martín L, Mazorra L. Site-adaptation of modeled solar radiation data: The SiteAdapt procedure. Remote Sens 2020;12:1–17. https://doi.org/10.3390/rs12132127.

[57] Vamvakas I, Salamalikis V, Benitez D, Al-Salaymeh A, Bouaichaoui S, Yassaa N, et al. Estimation of global horizontal irradiance using satellite-derived data across Middle East-North Africa: The role of aerosol optical properties and site-adaptation methodologies. Renew Energy 2020;157:312–31. https://doi.org/10.1016/j.renene.2020.05.004.
[58] Festa R, Ratto CF. Proposal of a numerical procedure to select Reference Years. Sol Energy 1993;50:9–17. https://doi.org/10.1016/0038-092X(93)90003-7.
[59] Carra E, Marzo A, Ballestrín J, Polo J, Barbero J, Alonso-Montesinos J, et al. Atmospheric extinction levels of solar radiation using aerosol optical thickness satellite data. Validation methodology with measurement system. Renew. Energy 2020;149:1120–32. https://doi.org/10.1016/j.renene.2019.10.106.
[60] Hiprahb EC. generation of typical meteorological years for 26 solmet stations. ASHRAE TRANS 1979;85:507–18.
[61] Wilcox S, Marion W. Users manual for TMY3 data sets. Renew. Energy 2008;51.
[62] Polo J, Fernández-Peruchena C, Gastón M. Analysis on the long-term relationship between DNI and CSP yield production for different technologies. Sol Energy 2017;155:1121–9. https://doi.org/10.1016/j.solener.2017.07.059.
[63] Kalamees T, Kurnitski J. Estonian test reference year for energy calculations, 2006, p. 40–58.
[64] Beccali M, Bertini I, Ciulla G, Di Pietra B, and Lo Brano V. SOFTWARE FOR WEATHER DATABASES MANAGEMENT AND CONSTRUCTION OF REFERENCE YEARS Department of Energy , University of Palermo , Palermo , Italy THE ISO 15927-4 METHODOLOGY. Proc. Build. Simul. 2011, Sydney: 2011.
[65] Blair N, Diorio N, Freeman J, Gilman P, Janzou S, Neises T, et al. System Advisor Model (SAM) General Description (Version 2017.9.5) 2018. https://doi.org/10.2172/1440404.
[66] Cruz NC, Redondo JL, Berenguel M, Álvarez JD, Ortigosa PM. Review of software for optical analyzing and optimizing heliostat fields 2017;72:1001–18. Doi: 10.1016/j.rser.2017.01.032.
[67] University of Wisconsin Madison. TRNSYS. TRNSYS, a Transient Simul Progr 1975. http://trnsys.com/index.html (accessed August 15, 2020).
[68] Wagner MJ, Wendelin T. SolarPILOT : A power tower solar fi eld layout and characterization tool 2018;171:185–96. Doi: 10.1016/j.solener.2018.06.063.
[69] Gamil A, Gilani SIU, Al-kayiem HH. Simulation of Incident Solar Power Input to Fixed Target of Central Receiver System in Malaysia. IEEE Conf Sustain Util Dev Eng Technol 2013;2013:92–7. https://doi.org/10.1109/CSUDET.2013.6739506.
[70] Benammar S, Khellaf A, Mohammedi K. Contribution to the modeling and simulation of solar power tower plants using energy analysis. Energy Convers Manag 2014;78:923–30. https://doi.org/10.1016/j.enconman.2013.08.066.
[71] Mutuberria A, Pascual J, Guisado MV, Mallor F. Comparison of heliostat field layout design methodologies and impact on power plant efficiency. Energy Procedia 2015;69:1360–70. https://doi.org/10.1016/j.egypro.2015.03.135.
[72] Sastry A, Duvenhage DF, Hoffmann JE. A Parametric Study of Heliostat Size for Reductions in Levelized Cost of Electricity. South African Sol Energy Conf 2016;2016:1–8.
[73] Gueymard CA. Irradiance Variability and Its Dependence on Aerosols. SolarPACES 2011.
[74] Blair N, Dobos AP, Freeman J, Neises T, Wagner M, Ferguson T, et al. System Advisor Model, SAM 2014 .1.14 : General Description 2014. Doi: 10.2172/1126294.
[75] Chaanaoui M, Vaudreuil S, Bounahmidi T. Benchmark of Concentrating Solar Power Plants: Historical, Current and Future Technical and Economic Development. Procedia Comput Sci 2016;83:782–9. https://doi.org/10.1016/j.procs.2016.04.167.
[76] Qaisrani MA, Wei J, Khan LA. Potential and transition of concentrated solar power: A case study of China. Sustain Energy Technol Assessments 2021;44:101052. https://doi.org/10.1016/j.seta.2021.101052.
[77] Water's High Heat Capacity n.d. https://bio.libretexts.org/Bookshelves/Introductory_and_General_Biology/Book%3A_General_Biology_(Boundless)/2%3A_The_Chemical_Foundation_of_Life/2.2%3A_Water/2.2C%3A_Water's_High_Heat_Capacity (accessed September 2, 2020).
[78] The Heat Capacity of Air is too Low to Heat Oceans of Melt Polar Ice n.d. http://nov79.com/gbwm/htcap.html (accessed September 2, 2020).
[79] Cohen G, Kearney D, Kolb G. Final report on the operation and maintenance improvement program for concentrating solar power plants 1999:1–44. Doi: 10.2172/8378.
[80] ToolBox E. Thermal Conductivity of selected Materials and Gases 2003. https://www.engineeringtoolbox.com/thermal-conductivity-d_429.html (accessed September 9, 2020).
[81] Deng H, Boehm RF. An estimation of the performance limits and improvement of dry cooling on trough solar thermal plants. Appl Energy 2011;88:216–23. https://doi.org/10.1016/j.apenergy.2010.05.027.
[82] Turchi CS, Wagner MJ, Kutscher CF. Water Use in Parabolic Trough CSP- Summary Results from Worley Parsons' Analyses 2010; Task No. S:108.
[83] Gilman P, Dobos A. System Advisor Model, SAM 2011.12.2: General Description 2012. Doi: 10.2172/1046896.
[84] Soomro, Mengal, Memon, Khan, Shafiq, Mirjat. Performance and Economic Analysis of Concentrated Solar Power Generation for Pakistan. Processes 2019; 7:575. Doi: 10.3390/pr7090575.
[85] Torresol Energy n.d. https://torresolenergy.com/en/gemasolar/.
[86] NREL. SAM Case Study: Gemasolar 2013:1–10.
[87] Quaschning V, Kistner R, Ortmanns W. Influence of direct normal irradiance variation on the optimal parabolic trough field size: A problem solved with technical and economical simulations. J Sol Energy Eng Trans ASME 2002;124:160–4. https://doi.org/10.1115/1.1465432.
[88] Musi R, Grange B, Sgouridis S, Guedez R, Armstrong P, Slocum A, et al. Techno-economic analysis of concentrated solar power plants in terms of levelized cost of electricity. AIP Conf Proc 2017;1850. Doi: 10.1063/1.4984552.
[89] Tahir S, Ahmad M, Abd-ur-Rehman HM, Shakir S. Techno-economic assessment of concentrated solar thermal power generation and potential barriers in its deployment in Pakistan. J Clean Prod 2021;293. https://doi.org/10.1016/j.jclepro.2021.126125.
[90] CSP Focus n.d. http://www.cspfocus.cn/en/ (accessed December 15, 2021).
[91] N.R.E.L. Website with the collaboration of Solar Paces n.d. https://solarpaces.nrel.gov/ (accessed December 15, 2021).
[92] Dersch J, Schwarzbözl P, Richert T. Annual yield analysis of solar tower power plants With GREENIUS. J Sol Energy Eng Trans ASME 2011;133:1–9. https://doi.org/10.1115/1.4004355.
[93] Li X, Jin J, Yang D, Xu N, Wang Y, Mi X. Comparison of tower and trough solar thermal power plant efficiencies in different regions of China based on SAM simulation. AIP Conf Proc 2019; 2126. Doi: 10.1063/1.5117545.
[94] Ouali HAL, Merrouni AA, Moussaoui MA, Mezrhab A. Electricity yield analysis of a 50 MW solar tower plant under Moroccan climate. Proc 2015 Int Conf Electr Inf Technol ICEIT 2015 2015:252–6. Doi: 10.1109/EITech.2015.7162978.
[95] Ali H, Alsabbagh M. Residential Electricity Consumption in the State of Kuwait. Environ Pollut Clim Chang 2018;02:1–7. https://doi.org/10.4172/2573-458x.1000153.
[96] Ansari M. Kuwait Utilities Sector Ind Res 2013:1–15.
[97] Al-Khayat M, Al-Rasheedi M, Gueymard CA, Haupt SE, Kosović B, Al-Qattan A, et al. Performance analysis of a 10-MW wind farm in a hot and dusty desert environment. Part 2: Combined dust and high-temperature effects on the operation of wind turbines. Sustain Energy Technol Assessments 2021;47. https://doi.org/10.1016/j.seta.2021.101461.
[98] Al-Rasheedi M, Al-Khayat M, Gueymard CA, Ellen Haupt S, Kosović B, Al-Qattan A, et al. Performance analysis of a 10-MW wind farm in a hot and dusty desert environment. Part 1: Wind resource and power generation evaluation. Sustain Energy Technol Assessments 2021;47. Doi: 10.1016/j.seta.2021.101487.